CHALMERS

Eulerian-Lagrangian Modeling of Particle Mixing in Gas Fluidized Beds

Master of Science Thesis of Master Degree Program of Innovative & Sustainable Chemical Engineering

AFARIDEH BABADOOST

Department of Chemical & Biological Engineering

Division of Chemical Reaction Engineering

CHALMERS UNIVERSITY OF TECHNOLOGY

Göteborg, Sweden, 2011

Eulerian-Lagrangian Modeling of Particle Mixing in Gas Fluidized Beds

Master of Science Thesis of Master Degree Program of Innovative & Sustainable Chemical Engineering

AFARIDEH BABADOOST

Department of Chemical & Biological Engineering

Division of Chemical Reaction Engineering

CHALMERS UNIVERSITY OF TECHNOLOGY

Göteborg, Sweden, 2011

MASTER'S THESIS 2011

Eulerian-Lagrangian Modeling of Particle Mixing in Gas Fluidized Beds

Master's Thesis in the Master's program of Innovative & Sustainable Chemical Engineering

AFARIDEH BABADOOST

Department of Chemical & Biological Engineering

Division of Chemical Reaction Engineering

CHALMERS UNIVERSITY of TECHNOLOGY

Göteborg, Sweden, 2011

Eulerian-Lagrangian Modeling of Particle Mixing in Solids-gas Fluidized Beds

Master's Thesis in the Master's program of Innovative & Sustainable Chemical Engineering

AFARIDEH BABADOOST

Master's Thesis 2011

Department of Chemical & Biological Engineering

Division of Chemical Reaction Engineering

CHALMERS UNIVERSITY of TECHNOLOGY

Göteborg, Sweden, 2011

SE-412 96 Göteborg

Sweden

Telephone: +46(0)31- 772 1000

Eulerian-Lagrangian Modeling of Particle Mixing in Solids-gas Fluidized Beds

Master's Thesis in the Master's Program Innovative & Sustainable Chemical Engineering

AFARIDEH BABADOOST

Department of Chemical and Biological Engineering

Division of Chemical Reaction Engineering

ABSTRACT

The diploma work concerns Eulerian-Lagrangian modeling of particle mixing in gas-solid fluidized beds. That has a great influence on the performance of fluidized-bed combustors. Better horizontal and vertical mixing yields homogenous cross-sectional tracer distribution in the furnace and secures long enough contact time between oxygen and the tracer particles. To understand the motion of the two particulate phases (inert bed material) suspended in a fluid, the Lagrangian particle tracking technique is used.

This study contains numerical modeling of mono disperse particles mixing in spouted beds and fluidized beds in different beds' dimensions. Formulating a suitable statistical procedure for analyzing the results obtained and results were evaluated based on schematic comparison of tracer particles' concentration and degree of mixing in specific regions of the bed; moreover, preferential position, which states about the general distribution and tendency of particles to move across the regions of bed during mixing time, velocity vector and horizontal dispersion patterns are obtained to investigate about the mixing in the beds.
The numerical study is done in open source software for simulating fluid dynamics of fluidized beds (MFIX), The code was developed at the National Energy Technology Laboratory (NETL), USA.

Key words: MFIX, Fluidized bed, Lagrangian simulation, Multiphase numerical modeling

Table of Contents

Preface

In this work, Eulerian- Lagrangian numerical modeling of mono dispersed mixing in fluidized beds is performed using MFIX open source software at Division of Fluid Mechanics at Department of Mechanical Engineering, Chalmers University of Technology, Sweden.

The diploma work is carried out from beginning of 2010 to beginning of 2011 by supervision of researcher, Meisam Farzaneh and advisor, Professor Srdjan Sasic at Department of Mechanical Engineering. Professor Bengt Andersson at Department of Chemical & Biological Engineering was examiner of this Master's Thesis work.

Finally, I would like to have special thanks to Prof. Srdjan Sasic and Meisam Farzaneh, PhD, for their useful comments and support of this work at Multiphase group in Division of Fluid Mechanics.

I am so thankful of my lovely parents and family and my loved one whom supported me by all means during studies and granted me the best encouragement.

Göteborg, Sweden, February 2011

Afarideh Babadoost

List of Figures

List of Tables

Nomenclature

Roman Upper Case Letters

C_d Empirical Drag coefficient

F_s Solid drag force

F_{sml} Drag coefficient between m^{th} and l^{th} solid phase

F_{gm} Drag coefficient between gas and m^{th} solid phase

$\overrightarrow{F_{coll}}$ Inter-particle collision force

$\overrightarrow{F_{coll}^{n}}$ Normal force

$\overrightarrow{F_T^{(\iota)}}$ Net sum of forces acting on the i^{th} particle

$\overrightarrow{F_c^{(\iota)}}(t)$ Total contact forces between particles

$\overrightarrow{F_d^{(\iota\in k,m)}}(t)$ Total drag force on i^{th} particle belonging to the in k^{th} cell and in the m^{th} solid phase

G_{12} Relative velocity at particle centroids

$\vec{I}_{gm}$ Interaction force of momentum transfer between gas and m^{th} solid phases

$\overrightarrow{I_{ml}}$ Interaction between m and l phases of solid (solid- solid momentum transfer)

$I^{(i)}$ Momentum inertia of i^{th} particle

$\vec{J}$ Impulsive force vector exerted on particle 1

$\vec{J}_{t,\ sliding}$ Sliding collision

$\vec{J}_{t,\ sticking}$ Sticking collision

N_m Number of particles in phase mth solid

N Total number of particles in Lagrangian tracking

P_{jm} Pressure of particle j in m^{th} solid phase

Re_p Particle Reynolds number

R_{gn} Mass transfer interphase

R_{smn} Mass transfer interphase

R_{ml} Mass transfer from m^{th} to l^{th} phases of solids

R_{0m} Mass transfer from gas to the m^{th} solid phase

$\overrightarrow{S_g}$ Gas phase stress tensor

$\overrightarrow{S_{sm}}$ m^{th} solid phase stress tensor

U_{pimj} Vvelocity of particle *i* of m^{th} phase in cell *j*

U_{smj} Volume averaged solid velocity of m^{th} solid phase in cell *j*

V_{smj} Total solid volume fraction of m^{th} solid phase in cell *j*

V_{pimj} Volume fraction of a particle *i* of m-th size solid phase in fluid cell *j*

V_j Cell volume

V_j Particle volume

V_m Total particles' volume in the cell

$\overrightarrow{V(t)^{(i)}}$ Particle's linear velocity

$\overrightarrow{X(t)^{(i)}}$ Particle's position

Roman Lower Case Letters

$d^{(i)}$ Particle *i* diameter

d_p Particle diameter

e_n Coefficient of normal restitution

e_t Coefficient of tangential restitution

$\overrightarrow{f_g}$ Internal porous surface force

k_n Stiffness factor

$m^{(i)}$ Mass of particle *i*

$\vec{n}$ Normal velocity

$\overrightarrow{n_{ij}}$ Unit normal between particle *i* to *j*

$\vec{t}$ Tangential velocity

Δt Computational time step

$\vec{u}$ Fluid velocity

Greek Letters

β Interphase momentum exchange coefficient

δ Overlap displacement

δ_{ij} Overlap displacement between particles *i* and *j*

ε_g Volume fraction of fluid phase (Void fraction)

ε_{sm} Volume fraction of m^{th} solid phase

ε_{smj} Volume fraction of particle *i* of m^{th} size solid phase in fluid cell *j*

ε_{sj} Total volume fraction in the cell

ε_j Volume fraction in j^{th} cell

ε_m Solid phase volume fraction

η Damping coefficient

μ_f Coefficient of friction

μ_g Fluid viscosity

ρ_g Fluid density

ρ_{sm} m^{th} solid phase density

$\rho^{(i)}$ Particle's density

υ_p^1 Particle velocity after collision with wall

$\overrightarrow{\upsilon_g}$ Fluid velocity

$\overrightarrow{\upsilon_{sm}}$ m^{th} solid phase velocity

$\overrightarrow{v_{12}}$ Relative velocity of particles *i* and *j*

$\overrightarrow{\omega(t)^{(\iota)}}$ Particle's angular velocity

1 Chapter One

1.1 Introduction

The purpose of this thesis is numerical modeling of Eulerian-Lagrangian solid particles mixing in fluidized bed with MFIX (Multiphase Flow with Interphase eXchanges). MFIX is multi-purpose software developed by National Energy Technology Laboratory (NETL), USA. MFIX is written in FORTRAN; it is a hydrodynamic modeling tool uses for chemical reaction and heat transfer modeling in various types of solid-fluid flows, dealing with energy and mass conservation, gives accurate time-dependant information on pressure, temperature, composition and velocity distribution of phases [1]. Stability, speed up calculation and accuracy in calculation are factors in high importance in every modeling. MFIX enhances two first factors by replacing old-iterating method with two modified extension of SIMPLE (semi-implicit scheme); first, to enhance the solid convergence when solids are poorly packed with help of equation of solids volume fraction correction instead of solids pressure correction. Second, uses automatic time-step alteration to enhance the highest speed executes. The latter factor, accuracy, discretization convection term is altered to the second-order upwind [2].

Gas-particle flow is a dominant concept on design and formulation of MFIX. Therefore, we review the governing solids-gas flow equations, particle and fluid tracking approach in Eulerian-Lagrangian framework, Discrete Element Simulation (DES), Drag force criteria, collision and etc. Following to that, computational method to solve practically formulations in designing and programming MFIX is discussed.

1.2 Gas-solid flows

The controversial concept of gas-solid flows is described by strong coupling between fluid and particles. Fluid flows through voids formed by solid particles. A drag force exerted mutually from gas to solids and from solids equally and opposite to the gas. Therefore, pressure gradient arises that makes press forces on the particle phases. This phenomenon accompanied with different density of phases which causes buoyancy driving flows, makes energy and momentum exchange between two phases.

1.3 Continuity & momentum equations

Hydrodynamic motions of gas -solid phases are defined by generalized spatially outlined Navier-Stokes equations for two-phase flow mixtures. Gas and solid continuity and momentum equations' description categorized in two definite groups of Eulerian-Eulerian and Eulerian-Lagrangian approaches, which are briefly and respectively, are discussed.

General gas continuity equation is:

$$\frac{\partial}{\partial t}(\varepsilon_g \rho_g) + \nabla.(\varepsilon_g \rho_g \overrightarrow{\upsilon_g}) = \sum_{n=1}^{N_g} R_{gn} \quad (1.1)$$

Solid continuity equation defined as for mth solid phase:

$$\frac{\partial}{\partial t}(\varepsilon_{sm} \rho_{sm}) + \nabla.(\varepsilon_{sm} \rho_{sm} \overrightarrow{\upsilon_{sm}}) = \sum_{n=1}^{N_{sm}} R_{smn} \quad (1.2)$$

The terms on the right side of equations (1.1) & (1.2) stand for mass transfer interphase due to chemical reaction and/or physical processes such as evaporation [3]. This term is zero in cases where there is no chemical process considered in the fluidized bed [4], [10].

Momentum equations used for gas phase in general form is:

$$\frac{\partial}{\partial t}(\varepsilon_g \rho_g \overrightarrow{\upsilon_g}) + \nabla.(\varepsilon_g \rho_g \overrightarrow{\upsilon_g} \overrightarrow{\upsilon_g}) = \nabla.\overrightarrow{S_g} + \varepsilon_g \rho_g \vec{g} - \sum_{m=1}^{M} \overrightarrow{I_{gm}} + \overrightarrow{f_g} \quad (1.3)$$

$\overrightarrow{S_g}$ represents gas phase stress tensor and $\vec{I}_{gm}$ is interaction force of momentum transfer between gas and mth solid phases, internal porous surface insert force of $\overrightarrow{f_g}$ [3].

Momentum equation for solid phase (mth solid phase) is:

$$\frac{\partial}{\partial t}\left(\varepsilon_{sm}\,\rho_{sm}\,\overrightarrow{\upsilon_{sm}}\right)+\nabla.\left(\varepsilon_{sm}\,\rho_{sm}\,\overrightarrow{\upsilon_{sm}}\,\overrightarrow{\upsilon_{sm}}\right)=\nabla.\overrightarrow{S_{sm}}+\varepsilon_{smg}\,\rho_{sm}\,\vec{g}-\sum_{l=0,l\neq m}^{M}\overrightarrow{I_{ml}}+\overrightarrow{I_{gm}} \quad (1.4)$$

In momentum equation of mth solid phase, $\overrightarrow{I_{ml}}$ is result of interaction between m and l phases of solid (solid- solid momentum transfer) as described by:

$$\overrightarrow{I_{ml}}=-F_{sml}\left(\overrightarrow{\upsilon_{sl}}-\overrightarrow{\upsilon_{sm}}\right)+R_{ml}\left[\xi_{ml}\overrightarrow{\upsilon_{sl}}+\bar{\xi}_{ml}\overrightarrow{\upsilon_{sm}}\right] \quad (1.5)$$

In equation (1.5), R_{ml} is mass transfer from mth to lth phases of solids and so, where $R_{ml}\geq 0$, then $\xi_{ml}=0$ and where $R_{ml}<0$ $\xi_{ml}=1$. Moreover, $\bar{\xi}_{lm}=1-\xi_{lm}$.

The major interaction forces in fluidized beds are drag force, buoyancy and momentum transfer caused by mass transfer. Solid-fluid interaction force concluded as:

$$\overrightarrow{I_{gm}}=-\varepsilon_{g}\nabla P_{g}-F_{gm}\left(\overrightarrow{\upsilon_{sm}}-\overrightarrow{\upsilon_{g}}\right)-R_{0m}\left[\xi_{0m}\overrightarrow{\upsilon_{sm}}+\bar{\xi}_{0m}\overrightarrow{\upsilon_{g}}\right] \quad (1.6)$$

In equation (1.6) the first term on right side is buoyancy, second is drag force and third term describes momentum transfer due to mass transfer between gas and solid phases, where R_{0m} describes the mass transfer from gas to the mth solid phase which split when $R_{0m}\geq 0$ then $\xi_{0m}=0$, and when $R_{0m}<0$ then $\xi_{0m}=1$. Similarly, $\bar{\xi}_{0m}=1-\xi_{0m}$.

To close the above equation, solid stress tensor is required but the formulation of kinetic theory used in MFIX is replaced by DES so, there is no need for this closure.

In favor of using DES, solids continuity equation and solids momentum equations are omitted. Continuum simulation is coupled with DES; so that, solids volume fraction and solids velocity are directly calculated in order to find the exact position and velocity of particles. As a result, particles should be located in each gas computational cell [3].

1.4 Solid-phase, Discrete Element Method (DEM)

In DEM simulation, particles are tracked individually. Particles are categorized and packaged based on diameters and densities so that create various solid phases. For example, m^{th} solid phase is individualized by N_m spherical particles with each particle in diameter d_m and density ρ_{sm}.

Summation total number of M solid phases gives the total number of particles, N, which represents Lagrangian approach:

$$N = \sum_{m=1}^{M} N_m \tag{1.7}$$

At time *t* these N particles which stated are representative of Lagrangian framework are referenced by set of vectors as { $\overrightarrow{X(t)^{(i)}}$, $\overrightarrow{V(t)^{(i)}}$, $\overrightarrow{\omega(t)^{(i)}}$, $d^{(i)}$, $\rho^{(i)}$, i = 1,…, N}. These vectors denote respectively as particle's position, particle's linear velocity and particle's angular velocity, $d^{(i)}$ represents particle's diameter and $\rho^{(i)}$ is particle's density. In Lagrangian tracking, density and diameter of each particle is same as m^{th} solid phase stated before.

Following equations are used to describe the mass ($m^{(i)}$) and momentum inertia ($I^{(i)}$)of the *i* th particle are respectively [10]:

$$m^{(i)} = \rho^{(i)} \pi \, (d^{(i)})^3 /6 \tag{1.8}$$

$$I^{(i)} = m^{(i)} (d^{(i)})^2 /10 \tag{1.9}$$

Based on the MFIX documentation, following equations are defined to calculate linearly the position and angular velocities of i^{th} particle, respectively [10]:

$$\frac{d\overrightarrow{X(t)^{(i)}}}{dt} = \overrightarrow{V(t)^{(i)}} \tag{1.10}$$

$$m^{(i)} \frac{d\overrightarrow{V(t)^{(i)}}}{dt} = \overrightarrow{F_T^{(i)}} = m^{(i)} \vec{g} + \overrightarrow{F_d^{(i\in k,m)}(t)} + \overrightarrow{F_c^{(i)}}(t) \tag{1.11}$$

$$I^{(i)} \frac{d\overrightarrow{\omega(t)^{(i)}}}{dt} = \overrightarrow{T^{(i)}} \tag{1.12}$$

Equation (1.11), $\overrightarrow{F_T^{(i)}}$ is net sum of forces acting on the i^{th} particle and consisted of gravity force, $\overrightarrow{F_d^{(i\in k,m)}(t)}$ which is the total drag force, consists of pressure and viscose forces on i^{th} particle

belonging to the in kth cell and in the mth solid phase; also, $\overrightarrow{F_c^{(i)}}(t)$ is total contact forces between particles.

Two main forces which dominates gas-solid motion are interphase drag and pressure force or buoyancy. Although, other interactive forces, such as, Basset force, Magnus lift force etc. could be considered.

1.4.1 Drag force

Drag force is a result of energy dissipation at the particle surface and corresponds to the fluid mean velocity related to that of the particle. Hoomans et al. and Kawaguchi et al. illustrate forces act on a single particle as [4], [6]:

$$m_p \frac{d\vec{v}_p}{dt} = m_p \vec{g} + \frac{\vec{v}_p \beta}{(1-)} (\vec{u} - \vec{v}_p) - \vec{v}_p \nabla p \qquad (1.13)$$

In equation (1.13), the second term represents drag force and β stands for an interphase momentum exchange coefficient is obtained by Ergun equation. Drag force in high Reynolds number follows by empirical correlations and becomes non-linear function of related fluid-particle velocities [5]. Hoomans et al. state β, for ε < 0.80, is [3], [4], [9]:

$$\beta = 150 \frac{(1-)^2}{} \frac{\mu_g}{d_p^2} + 1.75 (1- \varepsilon) \frac{\rho_g}{d_p} | \vec{u} - \vec{v}_p |$$

(1.14)

For low volume fraction, Ergun equation is not sufficient; therefore, for ε ≥ 0.8, Wen and Yu presented the following equation for C_d, which is an extension of Richardson and Zaki formulation [4]:

$$C_d = \frac{3 (1-)}{d_p} C_d \rho_g | \vec{u} - \vec{v}_p | \varepsilon^{-2.65} \qquad (1.15)$$

In empirical correlations, drag coefficient, C_d is a function of Reynolds number [4], [5], [7]:

$$C_d = \begin{cases} \frac{24}{Re_p} (1 + 0.15 \, Re_p^{0.687}) & Re_p < 1000 \\ 0.44 & Re_p \geq 1000 \end{cases} \qquad (1.16)$$

And particle's Reynolds number calculated as [4], [5], [7]:

$$Re_p = \frac{\rho_g \, |\vec{u} - \vec{v}_p| d_p}{\mu_g} \quad (1.17)$$

Kuipers et al. suggested a correlation for drag force on a single particle in a particulate flow [3], [8]:

$$F_s = 1/8 \, C_d \, \pi \, d_p^2 \, \rho_f \, \left| \vec{u} - \vec{v}_p \right| (\vec{u} - \vec{v}_p) f() \quad (1.18)$$

C_d and Re in equation (1.18) calculated based on equation (1.16). Different suggestions are made for f. Wen and Yu has suggested simple function of $f = \varepsilon^{-4.7}$, Felice correlation which introduces parameter α in calculation of $f = \varepsilon^{\alpha}$ and $\alpha = 4.7 - 0.65 \exp\left[- \frac{(1.5 - \log Re)^2}{2} \right]$ when $2 < Re < 500$. Happel introduced another correlation, $f = \frac{3 + 2(1-\varepsilon)^{\frac{5}{3}}}{3 - 4.5(1-\varepsilon)^{\frac{1}{3}} + 4.5(1-\varepsilon)^{5/3} - 3(1-\varepsilon)^2}$ [3].

In calculation of drag force utilized in MFIX, terminal velocity of the m^{th} solid phase is used.

In all above equations, term of volume fraction was used. Volume fraction of fluid continuum and solid phase needs to be calculated which is described later in Void Fraction section.

Grag et al. has stated about numerical errors happen in obtaining accurate value for intephase momentum transfer. They believe it could be arise to particle locations by approximation of fluid velocity at grid nodes. As a result, different numerical schemes suggested and manipulated in order to improve numerical algorithm for computation interphase momentum transfer [16].

1.4.2 Void fraction

Domain of fluid continuum phase is meshed to computational cells. Each particle enters and exits from each cell and total value of all particles volume in each cell is solid volume fraction. Total solid volume fraction of m^{th} solid phase in cell *j* represented by V_{smj} is calculated by following equation:

$$V_{smj} = \sum_i V_{pimj} \quad (1.19)$$

While V_{pimj} is volume fraction of particle *i* of m-th size solid phase in fluid cell *j*. When cell volume is $V_j = \Delta x \Delta y \Delta z$, corresponding volume fraction is:

$$\varepsilon_{smj} = \frac{Vsmj}{Vj} \quad (1.20)$$

V_j components are width of the cell in x-Cartesian direction, also in y and z directions. By summation each phase solid particle's volume fraction in the cell, the total volume fraction in the cell is obtained:

$$\varepsilon_{sj} = \sum_m V_{smj} \quad (1.21)$$

In view of the fact that sum of various solid void fraction and fluid volume fraction is equal to one, volume fraction in j^{th} cell obtained by:

$$\varepsilon_j = 1 - \varepsilon_{sj} \quad (1.22)$$

1.4.3 Solid-phase velocity calculation

In Lagrangian tracking approach, it is needed to calculate each particle size group velocity. This velocity is a factor in calculation drag force and should be computed in each fluid cell; therefore, at the end of solid time step, each particle's velocity in the cell is calculated and all averaged. In order to have representative of solid velocity in each cell, these velocities are averaged in each cell and stored in the cell center, and give volume averaged solid velocity of m^{th} solid phase in cell j according to the following equation:

$$U_{smj} = \frac{\sum_i V_{pimj} U_{pimj}}{V_{smj}} \quad (1.23)$$

U_{pimj} , is a velocity of particle i of m^{th} phase in cell j . This velocity as stated, stored at center of cell while numerical schemes use the face center value. Thus, the related neighbor cells' center velocity should be weighted averaged crossed the face.

1.4.4 Pressure Force/Buoyancy Calculation

At each fluid time step the fluid continuum equation is solved and fluid properties like pressure and velocity is obtained. This pressure exerted from fluid to each individual particle in the cell and stored in the cell center. For the particle j in m^{th} solid phase P_{jm} is given by:

$$P_{jm} = \varepsilon_m P_c \frac{V_j}{V_m} \quad (1.24)$$

Where,

$\varepsilon_m = \frac{V_m}{\Delta x \Delta y \Delta z}$ (1.25)

In (1.24), V_j is particle volume, V_m is total particles' volume in the cell and ε_m is the solid phase volume fraction.

1.5 Collision in Discrete Element Method

In DES approach, particle-particle interaction and particle-wall interaction is considerable and loss of kinetic energy due to inter-particle collision in non negligible. Two models "Hard Sphere Model" and "Soft Sphere Model" are two common approaches utilized. Hard sphere model is quasi-instantaneous binary collision based on event driven approach and soft sphere model is modeled with spring-dashpot model. DES is based on soft sphere model since it is more robust because of independence to the time step size from volume fraction.

Energy released during collision affects coefficient of restitution while restored in elastic deformation connected with normal and tangential displacement of contact points corresponding to the sphere's center [11].

1.5.1 Hard Sphere model

Particle-particle collision in this approach is inelastic and time step is established based on minimum collision time between each two pairs of particles. This is analogous to mean free path. This approach is more suitable for dilute systems since the time step is much smaller than denser systems where particles collide with each in very short time scale. Due to inelasticity of this approach, energy will be re-supplied to the system.

In hard sphere modeling, particles move in a defined path and trajectories till collision with other particles happen. *Figure 1.1* can visualize hard sphere model.

Figure 1.1 Particle-particle collision in hard sphere approach [3]

Hard sphere model is based on impulsive forces which are integration of forces acting on the particle versus time. Equations below can define modeling by hard sphere approach [9]. If two particles with velocities of υ_1 and υ_2 have relative velocity υ_{12} at contact point, then this velocity is defined as:

$$\overrightarrow{v_{12}} = (\overrightarrow{v_1} - \overrightarrow{v_2}) - (r_1\overrightarrow{\omega_1} - r_2\overrightarrow{\omega_2}) \times \vec{n} \tag{1.26}$$

In equation (1.26), $\overrightarrow{\omega 1}$ and $\overrightarrow{\omega 2}$ are angular velocities and r_1, r_2 are radii of particle 1 and particle 2. Normal and tangential velocities, $\vec{n}$ and $\vec{t}$ are calculated by:

$$\vec{n} = \frac{(\overrightarrow{x_1} - \overrightarrow{x_2})}{|\overrightarrow{x_1} - \overrightarrow{x_2}|} \tag{1.27}$$

$$\vec{t} = \frac{\overrightarrow{v_{12}^0} - (\overrightarrow{G_{12}^0} \cdot \vec{n})\vec{n}}{|\overrightarrow{v_{12}^0} - (\overrightarrow{G_{12}^0} \cdot \vec{n})\vec{n}|} \tag{1.28}$$

Where subscription 0 points out state before collision and G_{12} indicated relative velocity at particle centroids. Equations (1.29), (1.30), (1.31) and (1.32) are equations of motion for particles where I_1 and I_2 are introduced as moments of inertia and $\vec{j}$ is impulsive force vector exerted on particle 1. Followed, various coefficients important in hard sphere modeling with related formulas are introduced. These coefficients are coefficient of normal restitution e_n, coefficient of friction μ_f and coefficient of tangential restitution e_t.

$$m_1(\overrightarrow{v1} - \overrightarrow{v_1^0}) = \vec{j} \tag{1.29}$$

$$m_2(\overrightarrow{v2} - \overrightarrow{v_2^0}) = -\vec{j} \tag{1.30}$$

$$\frac{I_1}{r_1}(\overrightarrow{\omega_1} - \overrightarrow{\omega_1^0}) = \vec{j} \times \vec{n} \tag{1.31}$$

$$\frac{I_2}{r_2}(\overrightarrow{\omega_2} - \overrightarrow{\omega_2^0}) = \vec{J} \times \vec{n} \quad (1.32)$$

I with indices 1 and 2 is I = (2/5) ma^2 [12]. Coefficient of restitution, e_n calculates with equation (33):

$$\vec{J}_n = m_1 m_2 (1+ e_n) \frac{(\overrightarrow{v_{12}^0} . \vec{n})}{(m_1 + m_2)} \quad (1.33)$$

Coefficient of friction and coefficient of tangential restitution are representative of two collisions, "sliding" and "sticking". Conditions, in which these collisions are valid, specified by following equations:

$$\vec{J}_{t,\ \text{sliding}} = - \mu_f \ \vec{J}_n \qquad \text{if } \mu_f < \frac{2m_1 m_2 (1+ e_t)\overrightarrow{v_{12}^0} . \vec{t}}{7(m_1 + m_2)\vec{J}_n} \quad (1.34)$$

$$\vec{J}_{t,\ \text{sticking}} = - (1 + \ e_t) \frac{2m_1 m_2 \overrightarrow{v_{12}^0} . \vec{t}}{7(m_1 + m_2)} \qquad \text{if } \mu_f \geq \frac{2m_1 m_2 (1+ e_t)\overrightarrow{v_{12}^0} . \vec{t}}{7(m_1 + m_2)\vec{J}_n} \quad (1.35)$$

1.5.2 Soft Sphere model

In various studies the need of modeling collision with soft sphere model is discussed and numerical investigations in DEM modeling using soft sphere model validated with experimental modeling of particles behavior in gas fluidized beds. Rhodes et al. stated that soft sphere model consumes much CPU time when modeling large dense beds especially when simulating particles with large spring constants is performed [13]. Voigt model which models springs and dashpots that has ability to be used in contact point of several particles with one particle is investigated; while, integration time step should be particularly smaller than interactions of particles duration in this type of modeling [14].

Soft sphere modeling starts with calculation of contact force exerted on particle *a*, which is sum of all contact forces from contact list particles of this particle such as wall and all particles named *b*.

$$\vec{F}_{contact,a} = \sum_{\forall b \in contactlist} (\vec{F}_{ab,n} + \vec{F}_{ab,t}) \quad (1.36)$$

The right hand side parameters in equation (1.36) states, the normal and tangential forces respectively between particles *a* and *b*. The torque is dependent on tangential force and defined by equation (1.37) as below:

$$\vec{T}_a = \sum_{\forall b \in contactlist} (R_a \vec{n}_{ab} \times \vec{F}_{ab,t}) \quad (1.37)$$

It is always tried to describe contact mechanism by a model which reduces the calculation time while provides the procedure with high accuracy; the simplest model originally suggested by Cundall abd Strack [7]. This model describes contact force by linear-spring and dashpot model shown in *Figure 1.3*.

In this model, the normal contact force between particles *a* and *b* is described by combination of k_n, normal spring stiffness, $\vec{n}_{ab}$ the normal unit vector, η_n, the normal damping coefficient, $\vec{v}_{ab,n}$ the normal relative velocity and overlap, δ_n. The contact force between two particles *a* and *b* is:

$$\vec{F}_{ab,n} = -k_n \delta_n \vec{n}_{ab} - \eta_n \vec{v}_{ab,n} \quad (1.38)$$

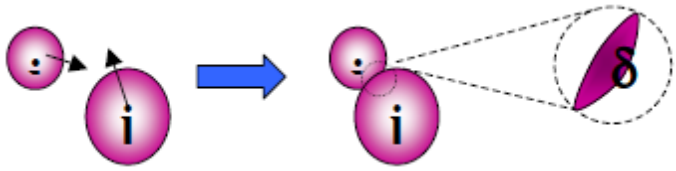

Figure 1.2 Particle-particle interactions in soft sphere model and displacement of δ [3]

Figure 1.2 shows the concept of displacement, δ_n, which is calculated as follows:

$$\delta_n = R_a + R_b - |\vec{r}_b - \vec{r}_a| \quad (1.39)$$

The normal relative velocity is calculates by equation (1.40):

$$\vec{v}_{ab,n} = (\vec{v}_{ab} \cdot \vec{n}_{ab})\vec{n}_{ab} \quad (1.40)$$

The normal damping factor acquired in calculation of normal contact force, is given by:

$$\eta_n = \frac{-2 \ln e_n \sqrt{m_{ab} k_n}}{\sqrt{\pi^2 + \ln^2 e_n}} \quad \text{if } e_n \neq 0 \quad \text{and } \eta_n = 2\sqrt{m_{ab} k_n} \quad \text{if } e_n = 0 \quad (1.41)$$

In equation (1.41), $m_{ab} = (1/m_a + 1/m_b)^{-1}$ and coefficient of normal restitution, e_n is defined as

$\vec{v}_{ab} \cdot \vec{n}_{ab} = e_n (\vec{v}_{ab,0} \cdot \vec{n}_{ab})$.

It is needed also to calculate the tangential force by its components of Coulomb-type friction law [7]:

$$\vec{F}_{ab,t} = -k_t \delta_t - \eta_t \vec{v}_{ab,t} \text{ when } |\vec{F}_{ab,t}| \leq \mu |\vec{F}_{ab,n}|$$

$$\vec{F}_{ab,t} = -\mu |\vec{F}_{ab,n}| \vec{t}_{ab} \text{ when } |\vec{F}_{ab,t}| > \mu |\vec{F}_{ab,n}| \quad (1.42)$$

Tangential spring stiffness, tangential displacement and tangential damping coefficient is described respectively as follows:

$$\eta_t = \frac{-2\ln\beta_0\sqrt{2/7m_{ab}k_t}}{\sqrt{\pi^2+ln^2\beta_0}} \quad \text{if } \beta_0 \neq 0, \text{ and } \eta_n = 2\sqrt{2/7m_{ab}k_t} \quad \text{if} \quad \beta_0 = 0 \tag{1.43}$$

In both components of equation (1.43), β_0 is the friction coefficient and its calculation is stated by Deen et al. (2007)[7]. The tangential displacement is described as:

$$\delta_t = \delta_{t,0}\vec{H} + \int_{t_0}^{t} v_{ab,t}\, dt \quad \text{if } |\vec{F}_{ab,t}| \leq \mu|\vec{F}_{ab,n}| \text{ and } \delta_t = \frac{\mu}{k_n}|\vec{F}_{ab,n}|\vec{t}_{ab} \quad \text{if } |\vec{F}_{ab,t}| > \mu|\vec{F}_{ab,n}| \tag{1.44}$$

Components of δ_t, such as$\vec{H}$ is defined in research work by Deen et al. (2007)[7].

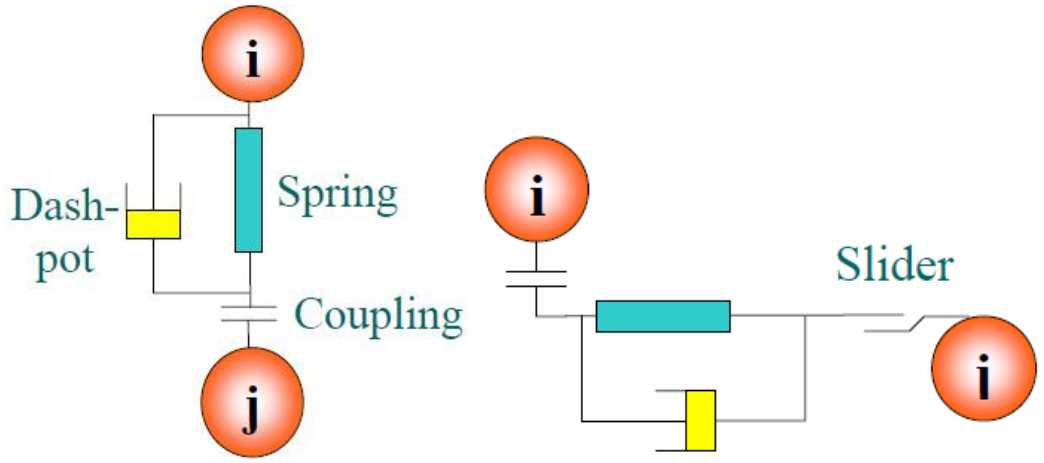

Figure 1.3 Spring dashpot model used in soft sphere model definition [3]

1.6 Particle-wall interaction:

Particle-wall interactions are considered as two particles' interaction with some modifications added, therefore, particle *j* is replaced by wall and $|\vec{v_j}| = 0$. One idea is to assume a reflecting wall. So, particle's velocity which contacted wall is related to coefficient of restitution. Initial velocity of particle in absence of wall is υ_p^0 and traveling distance of $\upsilon_p^0\Delta t$ after contact with wall and stay in domain. Δt_1 is time for particle travels to the wall and after collision will remain inside the domain after distance of $\upsilon_p^0(\Delta t - \Delta t_1)$. After contact, the velocity of particle is

$$\upsilon_p^1 = \upsilon_p^0 e \tag{1.45}$$

And total distance particle traveled would be $\upsilon_p^0\Delta t_1 + \upsilon_p^1(\Delta t - \Delta t_1)$. This idea is depicted in *Figure 1.4*.

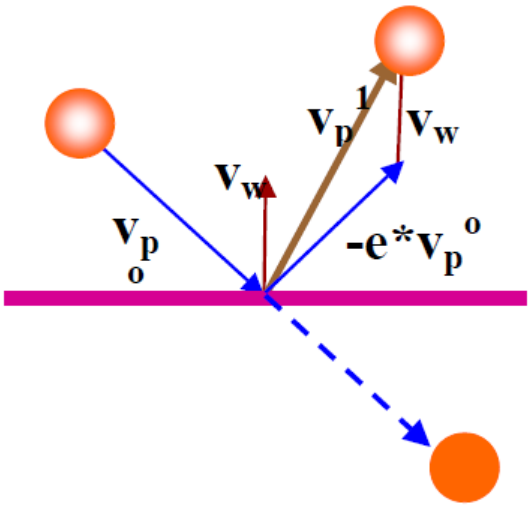

Figure 1.4 Particle-wall collision and corresponding velocities which related to coefficient of restitution [3]

Other suggestions of a scheme for particle-wall interaction are considered such as replacing neighbor *j* with wall. Another idea is periodic boundaries in large particle systems. Studies give another option such as "irregular bouncing" based on impulse equations for particle-wall interaction and gives higher value for particle velocity fluctuations which meets the experimental results better while movement of smaller particles are less affected by type of particle-wall collision model chosen [17].

1.7 Particle-neighborhood search

Collision detection is a sophisticated algorithm to find neighbor particles especially for large systems with wide range of particle size distribution. Some methods will be introduced in this section such as N^2 search, Quad-tree and Octree, No Binary Search, also other alternatives such as Verlet-Neighbor List (VL), Linked Cell (LC) and Linked Linear List (LLL) will be discussed.

1.7.1 N^2 search

This algorithm is the easiest way to search neighbors. The neighbors are found based on calculation the distance between particles, this approach utilizes $O(N^2)$ that N is the number of particles. It is not suitable for large-scale simulations due to expensiveness and generally is not recommended any more while other accurate methods uses now.

1.7.2 Quadtree and Octree search

This is hierarchical structure in 2D modeling and its 3D modeling concept is Octree. Recursively, Quadtree splits a cubic volume into four cubes which is eight in Octree procedure. These smaller cubes are called quadrants and Octants in 2D and 3D simulation respectively and divide until the decomposition norm achieved to get maximum resolution desired. Meshing method is producing equal size boxes to store the data. Using such grid method, unnecessary data will be stored but quadtree gives more promising results in storing data and operation. *Figure 1.5* shows one sample of quadtree meshing of a particle which is separate from effect of other particles. quadtree method is used for meshing the objects and providing O(NlogN) algorithm in subjective point neighborhood search.

In Octree method the query is arranging particles in quads which maximum of four particles could be allocated then searching for neighbors. This quad is known as parent quad. If fifth particle lies down in the quad then it divides to four sub-quads, called children quads and old particles allocate into new children quads. This procedure continues till a vacant position is found.

Next step is finding the neighbor. Therefore, a search region generates around the particles in a shape that all neighbor particles of interest should fall into this region and consequence of quadtree should be passed through and eliminating all the particles lay out of this search region. Therefore, in a moment that a quad meets the search region, the particles in quads start searching for neighbors.

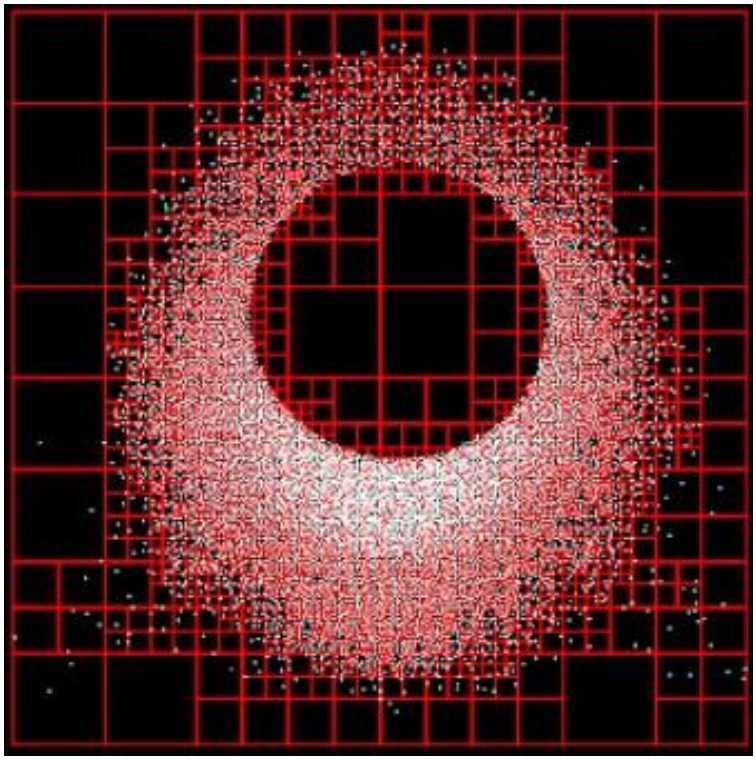

Figure 1.5 Sample of particle gridding in quadtree method of particle neighborhood search [http://www.flickr.com/photos/kylemcdonald/4096670086/in/photostream/]

In completion quadtree and octree particle neighborhood search, other methods are introduced for large amount of nodes stored in these methods [20]. Diffusion-limited Aggregation is an algorithmic structure used to determine the distance with help of DLA clusters with ability of distance searching between 10^9 in 2D simulation and 10^8 particles in 3D modeling. DLA upgraded to PDLA, a fractal cluster with ability of neighbor search among 10^{10} and 10^9 particles in 2D and 3D simulation respectively.

Algorithm in Diffusion-limited Aggregation is an iterative process that included of a seed particle in its origin in form of initial cluster. A particle far from the origin moves randomly toward the cluster, this particle is in distance usually called, birth radius, R_{bh}. It becomes part of the cluster when its distance to the origin is in a specific area. If the particles locate in boundaries exceeding R_{dh} then it is discarded. When certain number of particles established in the process, then it is ended. One challenge is that all particles in a cluster should be aware of other particles in the cluster and their distances [20].

1.7.3 No-Binary search

As per its name, No-binary Search is not engaged in any binary search and involved O (N) algorithm search. This algorithm is only suitable for systems of same-size particles [27]. The domain for neighbor searching first split in a cell which just one particle can fit into, then integrized into x, y and z zones and represented by ix, iy and iz coordinates. Only particles with integrized coordinate of ix-1, ix, ix+1, iy-1, iy, iy+1, iz-1, iz, iz+1 could be searched for neighborhood list.

Any combination of these integrized points could be detected to find neighbor particles. *Figure 1.6* shows a schematic overview of neighbor search in NBS method.

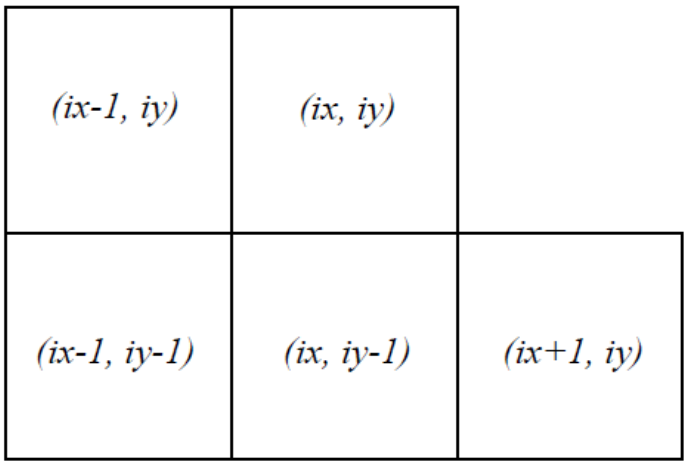

Figure 1.6 No-Binary Search method in finding neighbor cells [3]

Figure 1.7 shows a comparison between N^2 search algorithm, NBS, Quadtree and Octree neighbor search algorithms in 2D simulation for over 1000 particle size in logarithmic scale. Quadtree, octree and NBS are in some orders of magnitude quicker than N^2 searching method. While, NBS seems faster than quadtree and octree but since NBS is a searching method between particles of equal sized, in DES simulation quadtree and octree are more reliable for neighborhood searching.

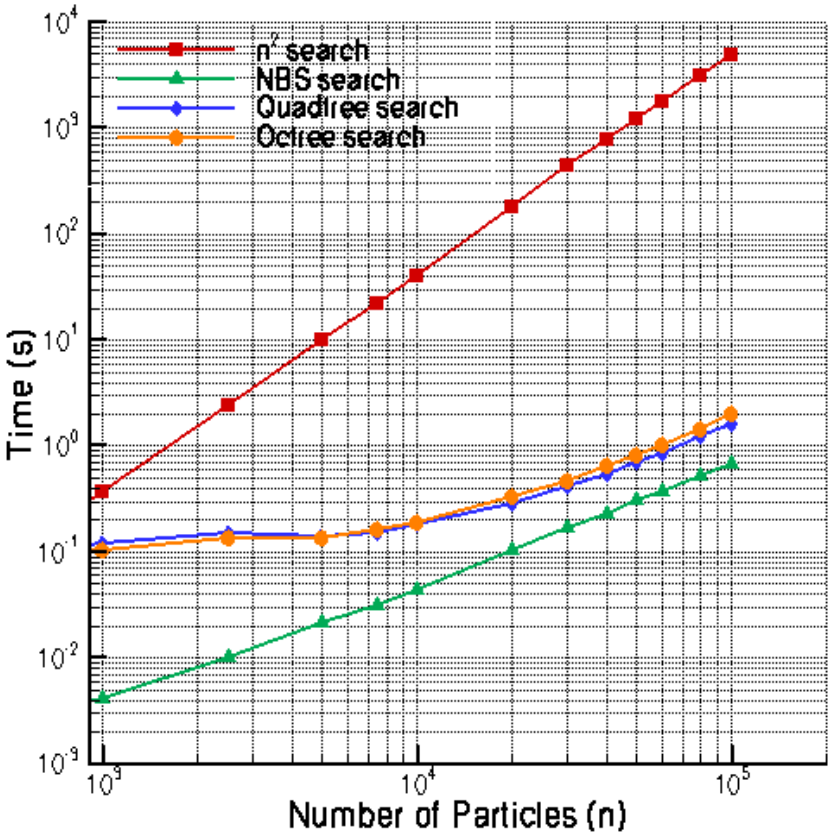

Figure 1.7 Comparison among N^2, NBS, Quadtree and Octree in 2D searching method for particle size more than 1000 [3]

Following to general-used algorithm discussed previously, other methods are also available for mostly large-scaled systems and preferably with different-sized particles that is discussed as follows [28].

1.7.4 Verlet-Neighbor List

In this method an imaginary sphere with radius of five times more than maximum particles' radius drawn [21]. It is shown in *Figure 1.8*.

Particles which fall in these spheres are considered as neighbor to the particle in the center of that sphere. Densities of the entire system in line with velocity of particles also, are key factors to determine the optimum extension of this zone. A list of neighbors created for each particle and particle of higher numbers than the body itself are tested regardless of their location inside or out of the sphere region. Therefore, n (n-1)/2 calculation steps are required and number of necessary

operation is still in order of O (n^2). The neighborhood list will not be updated and it depends on density of the system, sphere sizes and particles' velocity [21][22].

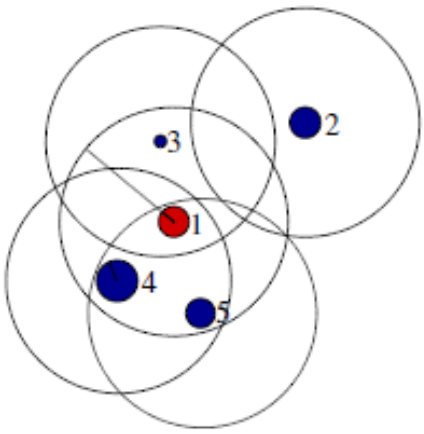

Figure 1.8 Verlet circles (2D)/spheres (3D) [21]

1.7.5 Linked-Cell (LC)

The domain is splited in to lattices like m×m×m cubic (3D).Non cubic lattice is also available. Optimal size of the cells are similar to VL method, described before but the imaginary cells are not attached to the particles and not moving with them [21][23]. In LC one cell can be determined that contains three particles. So, particles which are allocated in a same cell based on their position at the specific time interact with each other. (3^d +1) /2 cells will be examined for neighborhood which d=2 in 2D and d=3 in 3D cases. *Figure 1.9* shows LC method.

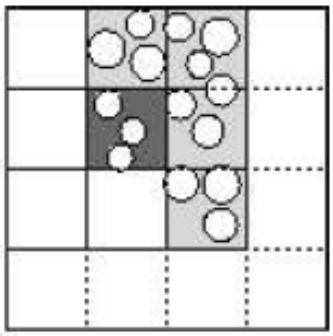

Figure 1.9 Linked cell methods in particle searching neighborhood [21]

1.7.6 Linked-Linear List (LLL)

Linked Linear List method is different from the last methods of VL and LC and it is a useful method to keep track of particles' neighbors in large body systems. Each particle is located in a box that exactly fits in and the sides of bounding boxes are lined with axis as shown in Fig…

In each time step particles location are projected on the x axis according to the length of their bounding boxes. *Figure 1.11* shows this projection for *Figure 1.10* each time step this projection differs. It happens a lot that beginning or ending or the whole projection of some particles overlap with others and in all time steps the overlapping calculations should be updated [21][24].

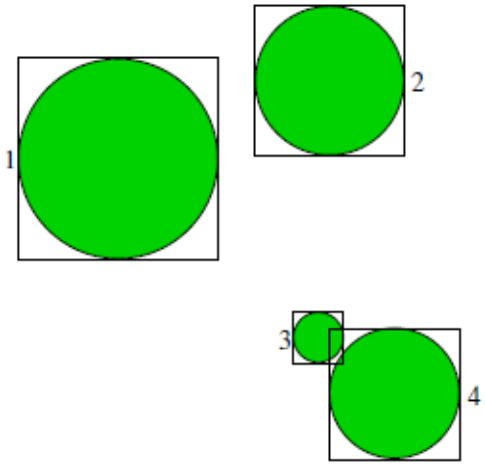

Figure 1.10 LLL bounding boxes contain various particles [21]

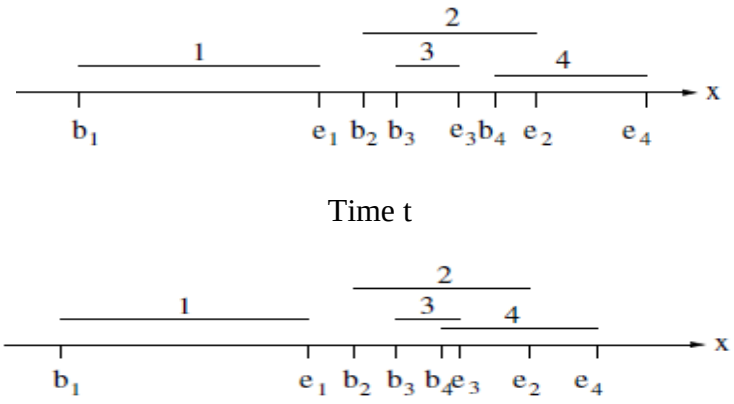

Figure 1.11 Particles' projection on x-axis in LLL neighborhood approach [21]

Particles' collision are determined based on the projection list and rules defined to identify the colliding particles when their projections interfere with each other and results of neighboring are stored in a sparse matrix where colliding bounding boxes are stored.

Further studies has improved Verlet-List and inked-Cell approaches and combined the advantages of both models to lower the computational time and iterations; also to reduce the construction of neighbor list .The result is an improved neighbor list in order of O (N); data sorting and algorithm of cell decomposition is arranged to reduce the time and maximize the speed and reducing the unnecessary operation in reconstruction the neighbor lists [25][26].

2 Chapter two: Solution method

This chapter describes the computational method used in MFIX 2.0, which is provided by MFIX Documentation Numerical Technique by Madhava Syamal (1998) [2].

To provide more stability and speed in computation, SIMPLE (SemiImplicit Method for Pressure Linked Equations) developed that utilizes automatic time-step adjustment for pressure-velocity coupling. Two major modifications done in new version of MFIX regarding use of SIMPLE method; first, when solids packed loosely, solid volume fraction correction equation helps convergence instead of solids pressure correction equation; moreover, in dense packed solids, this equation brings up with solids pressure. Second, the high speed performance guaranteed by automatic time-step modification.

Second-order upwind scheme is added to MFIX in order develop the precision in discretizing convection terms and error reduction (e.g. in predicting rounded shape for bubbles).

Finite volume is the numerical technique used in MFIX for the gas phase. The domain split to control volumes (CV) containing large number of particles that momentum, continuity equations, balance of energy and species exerted in CVs. MFIX utilizes structured mesh in 2D or 3D. Diffusion and convection terms solved by second-order upwind descritization scheme and various second-order limited method used for convection term. The value of all scalars is stored at cells' centroid, in addition to the gas and solids pressure. Gas and solids velocity is stored at cell face [3].

2.1 Convection-Diffusion term discretization

Convection-diffusion term in transport equation in 1D condition is defined as:

$$\frac{\partial(\rho u\phi)}{\partial x} - \frac{\partial\left(\Gamma\frac{\partial\phi}{\partial x}\right)}{\partial x} \tag{2.1}$$

Figure 2.1 shows control volume in x-direction. Integration this term over rectangular control volume gives:

$$\int\left[\frac{\partial(\rho u\phi)}{\partial x} - \frac{\partial\left(\Gamma\frac{\partial\phi}{\partial x}\right)}{\partial x}\right]dV = [\rho u\phi_{e-}(\Gamma\frac{\partial\phi}{\partial x})_e]\,A_e - [\rho u\phi_{e-}(\Gamma\frac{\partial\phi}{\partial x})_w]\,A_w \tag{2.2}$$

Which second-order accuracy scheme uses to calculate the diffusive flux at the east face according to equation (2.3)

$$(\Gamma\frac{\partial\phi}{\partial x})_e = \Gamma_e\frac{(\phi_E-\phi_P)}{\delta x_e} + O(\delta x^2) \tag{2.3}$$

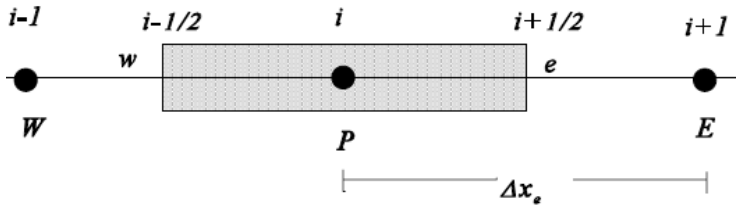

Figure 2.1 control volume and node locations in 1D, x-direction [3]

Value of ϕ at convection term is written as in equation (2.4) at east face and at west face according to equation (2.5):

$$\phi_e = (\xi_e \phi_E + \overline{\xi_e} \phi_P) \tag{2.4}$$

$$\phi_w = (\xi_w \phi_W + \overline{\xi_w} \phi_P) \tag{2.5}$$

ξ_e is weighting factor, that $\overline{\xi_e} = 1 - \xi_e$, value for weighting factor differs when $u_e \geq 0$ then $\xi_e = 0$ and when $u_e < 0$, $\xi_e = 1$ and consequently, $\overline{\xi_w} = 1 - \xi_w$ when $u_w \geq 0$ then $\xi_w = 0$ and when $u_w < 0$, $\xi_w = 1$.

2.2 Scalar transport equation discretization

Scalar ϕ in transport equation should be descritized and all terms, convection, diffusion and transient term in equation (2.6) should be integrated over control volume.

$$\frac{\partial(\rho_{mm}\phi)}{\partial t} + \frac{\partial(\rho_{mm} v_{mi}\phi)}{\partial x_i} = \frac{\partial\left(\Gamma_\phi \frac{\partial \phi}{\partial x_i}\right)}{\partial x_i} + R_\phi \tag{2.6}$$

The complete integrated form of each term is described in literatures; such as, calculation of diffusive fluxes at east face and use set of a harmonic mean of values for cell center calculation [3].

2.3 Source term

Generally, source terms are nonlinear and become linear as in equation (2.7), in this equation for stability reason, $R_\phi' \geq 0$.

$R_\phi \approx \overline{R\phi}$ - $R_\phi'\ \phi_P$
(2.7)

Integration equation (2.7) over control volume gives equation (2.8) and further combination and rearrangement gives equation (2.9) for ϕ.

$$\int R\phi\ dV = \overline{R\phi}\Delta V\ -\ R\phi'\ \phi_P \Delta V \quad (2.8)$$

$$a_P\phi_P = \sum_{nb} a_{nb}\ \phi_{nb}\ + b \quad (2.9)$$

nb represents as E,W,S,N,T and B. Discretized continuity equation multiply by ϕ needed to be subtracted from equation (2.9); therefore, set of coefficients defined as below:

$$a_E = D_e - \xi_e(\rho_{mm})_E\ (u_m)_e\ A_e \quad (2.10)$$

$$a_W = D_w + \overline{\xi_e}(\rho_{mm})_W\ (u_m)_w\ A_w \quad (2.11)$$

$$a_N = D_n - \xi_n(\rho_{mm})_N\ (\upsilon_m)_n\ A_n \quad (2.12)$$

$$a_S = D_s + \overline{\xi_s}(\rho_{mm})_W\ (\upsilon_m)_s\ A_s \quad (2.13)$$

$$a_T = D_t - \xi_t(\rho_{mm})_T\ (w_m)_t\ A_t \quad (2.14)$$

$$a_B = D_b + \overline{\xi_b}(\rho_{mm})_B\ (w_m)_b\ A_b \quad (2.15)$$

$$a_P = \sum_{nb} a_{nb}\ + a_p^0 + R\phi'\ \Delta V \quad (2.16)$$

$$b = a_p^0\ \ \phi_P{}^0\ \ +\ \ \overline{R\phi}\Delta V \quad (2.17)$$

$$a_p^0 = \frac{(\rho_{mm})^0}{\Delta t}\ \Delta\ V \quad (2.18)$$

Therefore, the diffusion contribution achieves as

$$D_e = \frac{(\Gamma_\phi)_e A_e}{\Delta x_e} \quad (2.19)$$

Consequently, the concluding discretized form of diffusion is:

$$a_P\phi_P = \sum a_{nb}\ \phi_{nb}\ + b \quad (2.20)$$

To increase stability in computation procedure, under-relaxation changes during iteration should be provided for field variables as described in equation (2.21):

$$\frac{a_P}{\omega_\phi}\phi_P = \sum_{nb} a_{nb}\,\phi_{nb} + \mathrm{b} + \frac{(1-\omega_\phi)}{\omega_\phi}\ \mathrm{a_P}\phi_P^{\,*} \qquad (2.21)$$

That, $0 < \omega_\phi < 1$.

Set of linear equation solvers are suggested in MFIX; such as, conjugate gradient and GMRES solvers with preconditions [3].

2.4 Solution algorithm summarize

Nature of gas-solid is unstable. In most of the cases, the transient modeling and results are time-averaged. If the time step is too large, the transient simulation diverges and too slow time step makes simulation slow. So, MFIX automatically adjusts the time step [2]. A computational technique outline is suggested for each fluid time step [3]:

1. At the start of time step, rates of reactions, physical properties and also, exchange coefficients should be computed
2. Based on current pressure field, $u_m^*, w_m^*, \upsilon_m^*$, fluid velocity field should be computed
3. P'_g stands for fluid pressure correction calculated
4. Under relaxation applied to renew field pressure; $P_g = \omega_{pg}\, P'_g + P^*_g$
5. In this step, using fluid pressure correction P'_g, fluid velocity field updates as: $u_m = u_m^* + u_m'$
6. Numerous gas phase iteration is needed to fulfill the appropriate convergence criterion
7. Now, DES-sub stepping starts; multiple solid time steps is utilized for a single fluid time step. Then at each solid time step following procedure should be completed:
    a) Calculation of contact forces; particles-wall interaction and inter-particles interactions
    b) Gas drag force exerted on every single particles should be computed
    c) Calculation of pressure force on every particles completes
    d) For each particles, new position, new velocity and acceleration computes
8. Now, the DES-sub stepping is over; with the results, solids volume fraction and void fraction in each computational cell computed. Solids velocity also calculated and the obtained results should be fed into MFIX.
9. Drag force applied from solids on the fluid should be calculated through gas-phase source term in this step
10. By achieving simulation time step, simulation stops otherwise it starts over from Step 1.

Convection terms should be discretized accurately, stable and have less oscillation. In order to have higher accurate and fewer spurious oscillation, a limiter is added to the discretization scheme; such as, second order scheme, third order accurate scheme ultraquick, Smart, Superbee, Muscl, Van Leer, Minmod, FPFOI, etc. are added to MFIX[37][38]. Superbee is a higher order scheme chosen due to its ability to predict the rounded shape of bubbles but the CPU time requirement for Superbee is the highest among other limiters stated above specially has given better results than second order discretization scheme.

3 Chapter Three: Results and discussions

In this work numerical investigation of mono dispersed systems of spherical particles, in a flatten-bottom spouted bed and then in a fluidized bed is performed. Tracer particles and bed materials have the same diameter but slightly different density. Numerical modeling of beds are two dimensional with different cross-sections of beds, 11 m, 15cm and 21cm with 0.50m height. The results are obtained by simulation with MFIX codes (Multiphase Flow with Interphase eXchange). The results will be compared with the visual, experimental study on spouted bed by Jin et al[29].

Spouted bed is categorized as a nonconventional fluidized bed. Some important parameters in modeling a spouted bed are minimum spouting velocity, spouted diameter and ratio of nozzle-to-particle diameter (D_i/d_p), etc. Also, Sphercity and internal angle of friction are influential parameters in particle size distribution [30]. Number of particles, position of particles and preferential arrangement of the particles in binary systems can improve the mixing efficiency of fluidized beds [31].

This work divided to four main parts; part one, sampling method, part two, particle concentration and mixing index, part three, general pattern-influence of spouting gas velocity, part four, general pattern-influence of fluidizing velocity. Figure 1.3 is a simple schematic view of the flatted-bottom spouted bed and fluidized bed used in the simulation.

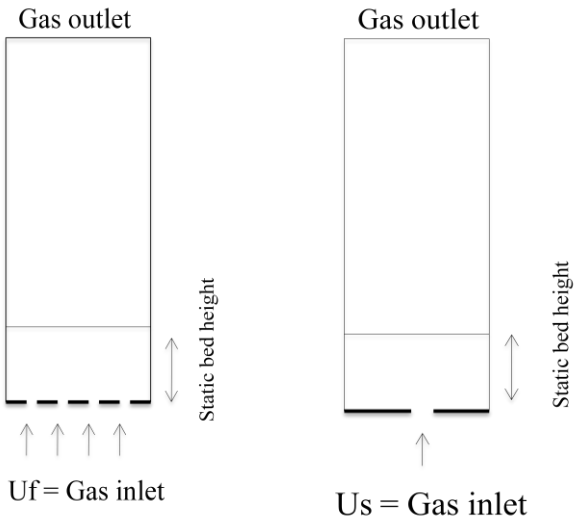

Figure 3.1 simple schematic view of the flatted-bottom spouted bed and fluidized bed used in the simulation

3.1 Sampling method

The solid particles' peculiarities manipulated as the bed material in the simulation are presented in the *Table 3.1*.

Table3.1 Physical properties of solid bed materials set in MFIX simulation

Diameter, d_p(m)	Density,ρ_p(kg/m^3)	Voidage, ε	Restitution coefficient
0.0028	900	0.42	0.96

Boundary conditions set in the modeling divide the whole bed to six sections; Distribution flow inlet at bottom that divides to three parts (gas-distributor plate at left, central jet, gas-distributor plate at right), the left side wall and right side wall and the exit at the upside of the bed. The dimensions of the bed mentioned before will satisfy the boundaries and 1 cm is considered for the central jet size. Initially, in the state of no air flow, the bed consisted of two layers of particles. Boundary conditions at distributor flow inlet, central gas jet which is located at the bottom of the bed (see *Figure 3.1*) is Mass inflow, at exit where located at top of the bed is Pressure outflow and at walls are Free slip wall.

For better understanding of the mixing behavior of particles with inspiration of the experimental sampling method in spouted-bed used by Jin et al [29], the numerical sampling method elaborated based on the location of each particles saved during the mixing process. Data of all particles' location are available every one second. Tracer particles' position is also saved every 0.01 second, then the particles Cartesian (x,y) location is ready to use in the formulations which could give the particles' concentration in specific areas in the bed.

Axial and radial tracer particles' concentration investigated. *Figure 3.2* can help to identify the locations where particles included bed materials and tracers were detected [29].

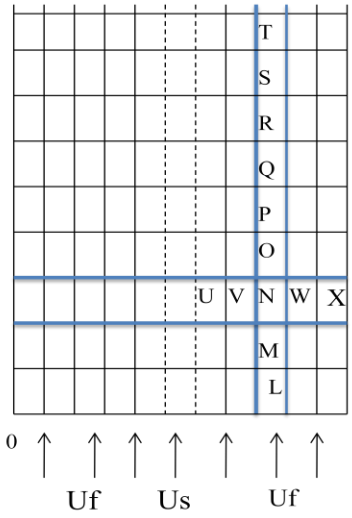

Figure 3.2 Schematic view of sampling regions corresponding to the tracer areas in the bed

Blocks which are marked with alphabetic characters are specified to detect the particles in. Each block has width and length of 0.01m×0.02m. The regions U, V, N, W, X is located horizontally.

3.2 Particle concentration & Mixing Index

Two parameters are important to calculate the concentration of particles; one, concentration of local tracer particles (c_{li}) and second, concentration of tracer particles (c) [29]. According to Jin et al. (2009):

$$c_{li} = \frac{n_i}{n_{it}} \tag{3.1}$$

$$c = \frac{n_i}{n_t} \tag{3.2}$$

Which n_i represents number of tracer particles in a sampling cell, n_{it} shows total number of particles in a given sampling cell and n_t gives total tracer particles in the whole bed [29].

The mixing index employed by Jin et al. [29] used to define the degree of mixing, is given in equation (3.3), although various mixing indices are defined for this purpose [33]. So that, mixing index, M is defined the ratio:

$$M = \frac{\sigma(c)}{\bar{c}} \tag{3.3}$$

Which, σ (c) represents standard deviation that is function of local tracer particles' concentration, therefore defined as:

$$\sigma\,(c_{li}) = \sqrt{\frac{\sum_{i=1}^{m}(c_{li}-\bar{c})}{m}} \tag{3.4}$$

Where, *m* represents number of sampling cells in the desirable system. $\bar{c}$ is average concentration of tracer particles in the bed. The amount obtained is approximately 0.1, which is observed in the plot of c_l vs. time, *Figure 3.2*.

Through the simulation, different gas velocities are applied and effect of increasing velocity on various bed dimensions and tracers' distribution and other results investigated. These velocities are calculated based on minimum spouting gas velocity (U_{ms}) and minimum fluidization velocity (U_{mf}) in equations (3.5) and (3.6)[30].

$$U_{ms} = \left(\frac{d_p}{D}\right)\left(\frac{D_i}{D}\right)^{1/3}\sqrt{\frac{2gH(\rho_p-\rho_f)}{\rho_f}} \qquad \text{for D<0.5 m} \tag{3.5}$$

$$U_{mf} = 0.00061\,\frac{g(\rho_p-\rho_f)d_p^2}{\mu_g} \qquad \text{for Ar <1000 and } Re_{mf}=6.1\times 10^{-4}Ar \tag{3.6}$$

In equation (3.5), D stands for bed width and H is considered as unit height. In equation (3.6), Ar number calculates based on Ar = $\frac{g(\rho_p-\rho_f)\rho_g d_p^3}{\mu_g 2}$ that in our simulation case is less than 1000.

3.2.1 Case1: Mixing process illustration

To have visual and mathematical observation of particles mixing and flow pattern of bed materials, especially tracer particles, which act an important role in mixing of bed materials and segregation, a modeling performed with specifications of U_f = 0 m/s, U_s =1.4 U_{ms}, the data obtained from this simulation could help to evaluate the mixing pattern of tracers by plot of mean concentration of local tracer particles by time. The sampling is done in three regions referred as U, N, X (*Figure 3.2*).

Figure 3.3 illustrates various stages in mixing particles. According to this plot, with respect to time, mixing process could be separated into three sections.

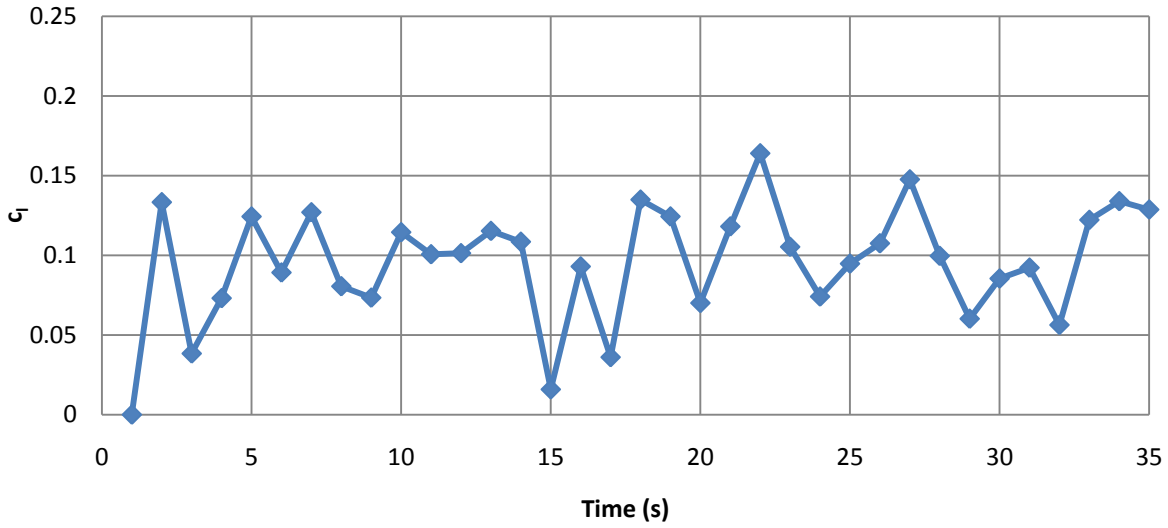

Figure 3.3 Mixing procedure and variation of mean concentration of tracer particles with time in cells U, N, X

With deeper notice, three sequential mixing stages could be distinguished. Macro-mixing, Micro-mixing and Stable-mixing stage [29]. Details of these stages are as following:

1. Macro-mixing stage, which the spouted jet gas begins to penetrate into the bed, mixing is limited to the region inside the jet (internal jet). From *Figure 3.2*, a rapid steep of mean concentration from the beginning of mixing to 0.1 mean concentration which is referred to the average point of the tracers' mean concentration. After 2 s of mixing, sudden falling off mean concentration detected which is followed by more slight steeps and change of mean concentration, and continues till mixing time of 10 s. velocity of mixing is high in this stage.

2. Micro-mixing stage, in which large particles mix with the bed materials. Driving force for this stage is spouted gas which penetrates through the whole bed and forms continuous circulation of particles. Dynamic equilibrium is close to reach in the next stage after micro-mixing stage ends in 15 s of mixing so this stage took 5 s.

3. Stable-mixing, forms after 15 s of mixing and steady state mixing observes. Degree of mixing basically does not change with time as in *Figure 3.2* the fluctuations after 15 s which are strong but around the average amount of mean concentration of local tracers. This figure shows the dynamical equilibrium reaches after 15 s.

It is worthy to notice that these results evaluate MFIX ability in modeling a spouted bed which is studied by Jin et al.[29]. Their results show 6 s of Macro-mixing stage and 6 s duration of Micro-mixing stage and finally the bed reaches dynamical state after 12 s.

Mostoufi & Chauoki [31] discussed mixing mechanisms and diffusivity in gas-solid fluidized beds. They described mixing of solid particles is underlying different mechanisms; Global mixing of solids which is caused by bubble-induced mixing that solid circulation occur due to the rising and bursting gas bubbled . Local mixing that is caused by random movement of solid particles.

3.2.2 Case 2: Effect of various spouting gas velocity at distribution of tracer particles' concentration

The axial distribution of tracer particles' concentration with different spouting gas velocities are shown in *Figure 3.4a*, *Figure 3.4b*, and *Figure 3.4c*. As shown, the results are obtained along the bed height in regions of L, M, N, O, P, Q, R, S, T in *Figure 3.2*; at vertical coordinate the concentration of tracer particles calculated based on equation (59). In this case, there is no fluidized gas velocity (u_f = 0 (m/s)) and spouting gas velocities at Us/U_{ms} = 1.2, Us/U_{ms} = 1.4, Us/U_{ms} = 1.6. This evaluation is done in different bed widths of 11cm, 15cm and 21cm.

In the lowest spouting gas velocity equals to minimum spouting gas velocity, generally amount of tracers' concentration is higher in annulus region rather than fountain region.

L, M, N, O and P are annulus regions; A dense region where is surrounding the spout and particles fall down in this region [29]. The rest of the referred regions are in fountain region where particles' concentration is very low.

According to *Figure 3.4a*, when the gas velocity rises up to $1.4u_{ms}$, concentration decreases more in annulus region in compare with the lower velocity (U_s=$1.2U_{ms}$) and as it goes to the upper region, the fountain area, where, concentration increases. As velocity goes to U_s= $1.6U_{ms}$, this trend particularly becomes infirm. The range of c (statically is the difference between minimum and maximum of a value) for different velocities implies that increasing in spouting gas velocity does not necessarily make increase in promotion axial mixing and shows an optimum for amount of increasing in spouting gas velocity. In *Figure 3.4a*, the lowest velocity has the highest value of concentration and after that the highest velocity shows higher concentration in various areas of the bed, but the general pattern remains same through different velocities that closer to the bottom bed shows more averaged concentration and as the vortexes in the bed, which bring particles upward, develop upward through bed, the concentration of particles decreases. This pattern is also applicable for *Figure 3.4b* and *Figure 3.4c*. By increasing the bed width which means increasing bed material in *Figure 3.4b*, the highest average concentration decrease in compare with *Figure 3.4a*. It could be interpreted that as the bed dimension increases in the same velocities, less particles pass across the same region in bed because they have more area to move so the concentration in specific areas of bed decreases by increasing the bed width and bed material. This conclusion makes sense when the bed width

increases further to 21 cm in *Figure 3.4c*, that at the same velocity, the average concentration in *Figure 3.4c* is less than *Figure 3.4b* and *Figure 3.4a*.

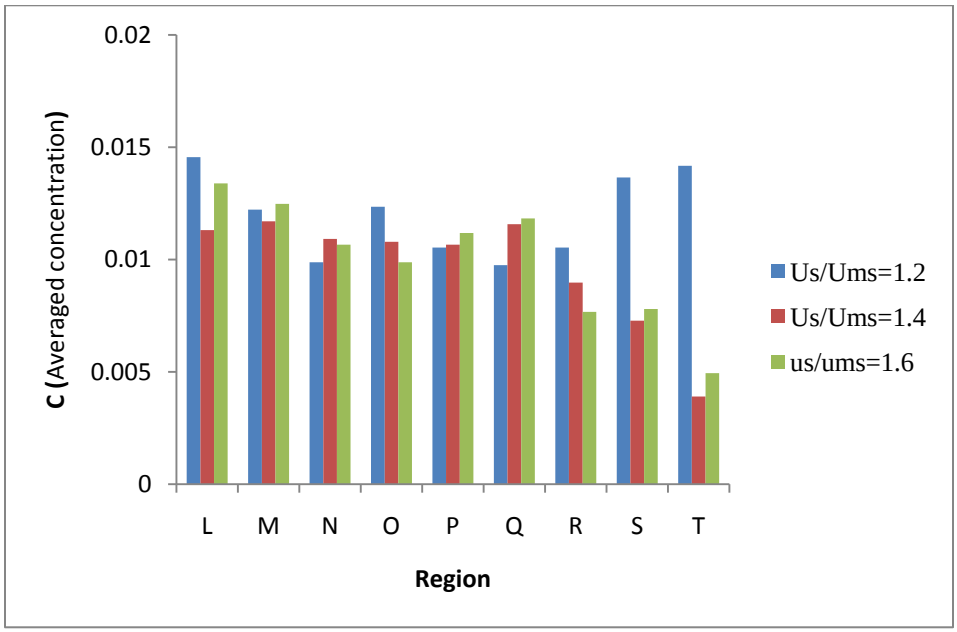

Figure 3.4a Axial distribution of tracer particles' concentration in spouted-bed with 11cm width at different spouting gas velocities

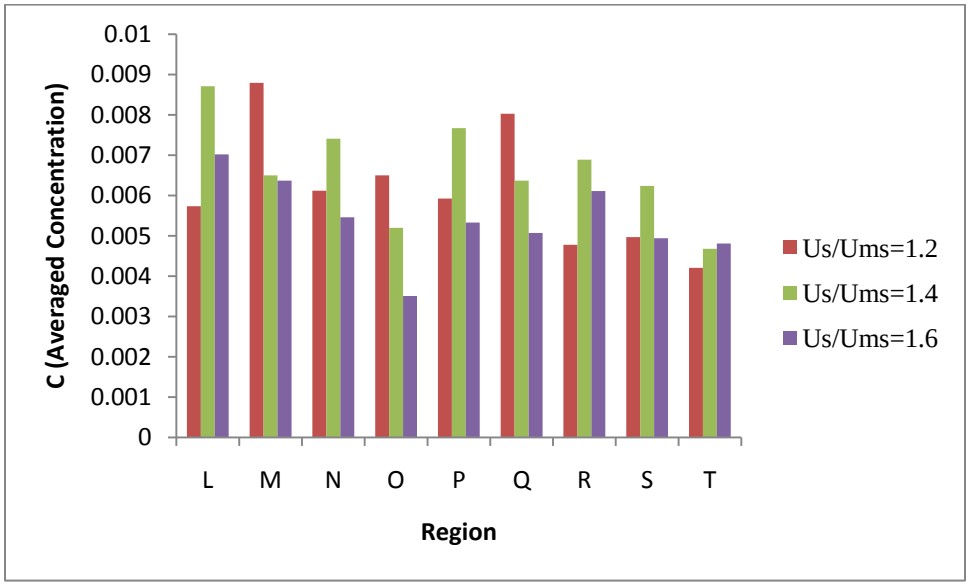

Figure 3.4b Axial distribution of tracer particles' concentration in spouted-bed with 15cm width at different spouting gas velocities

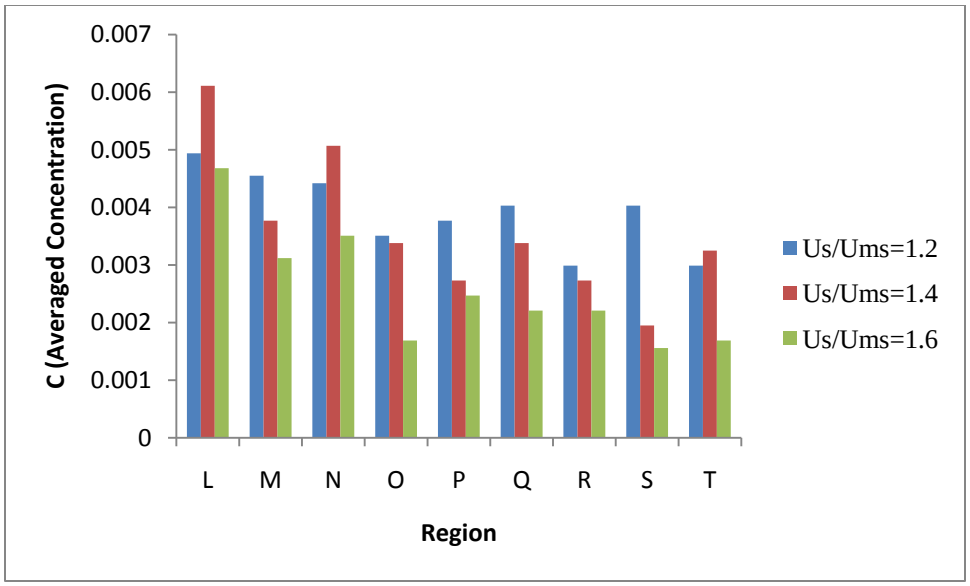

Figure 3.4c: Axial distribution of tracer particles' concentration in a spouted-bed with 21cm width at different spouting gas velocities

Radial distribution of tracer particles is another factor to better understand the behavior of spouted beds and fluidized beds beside axial distribution of tracer particles. Radial distribution of tracers' concentration in specific areas of U, V,N , W and X (according to *Figure 3.2*) is presented in *Figure 3.5a,3.5b* and *3.5c*.

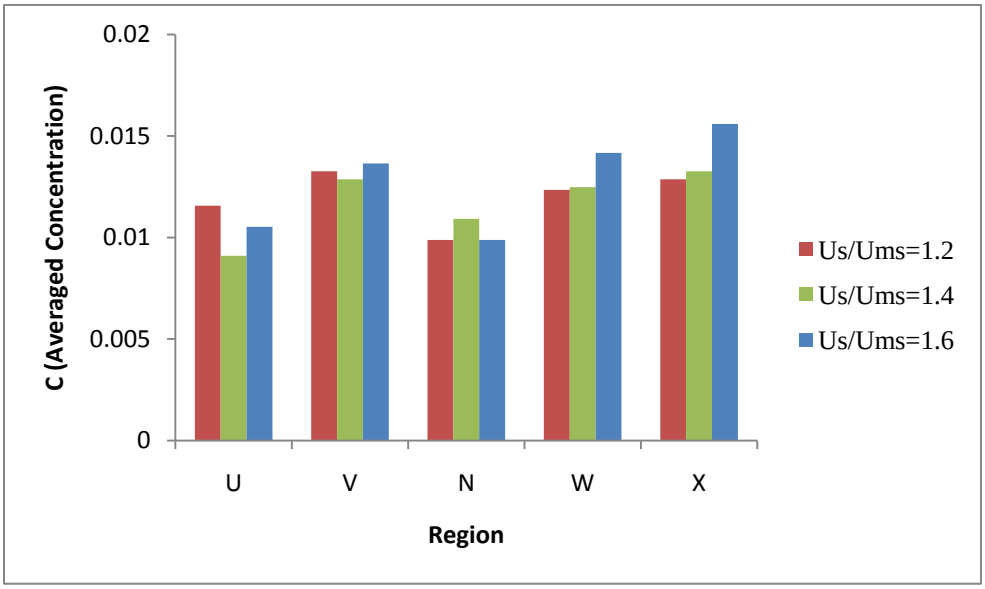

Figure 3.5a Radial distribution of tracer particles' concentration with various spouting gas velocities in spouted-bed with width of 11 cm

As per of *Figure 3.5a*, it is expected to have more concentration in region V. Slight increase in the concentration of tracers distinguishable from region U to X in U_s/U_{ms} =1.2 that higher concentration is in region X, near wall. It is difficult to compare the results by axial and radial mixing, but obviously increasing spouting bed, increases degree of mixing in spouted bed.
According to *Figure 3.5a*, as the sampling region moves closer the wall side, the tracers' concentration increases. The highest value of concentration in radial distribution is observed in highest spouting velocity. The mentioned pattern is also observable in *Figure 3.5b*, the concentration distribution is less uniform than *Figure 3.5a*, and the highest value is this case is less than in *Figure 3.5a*. It may due to the fact that by increasing bed width, fewer particles may move across specific sampling areas in the bed, so the concentration of tracer particles decreases by increasing the bed width. As the velocity increases, more uniform tracer concentration distribution is observed in the bed. It makes sense in *Figure 3.5c* as well that by increasing bed width, the average concentration decreases in sampling regions. More uniform distribution of tracers' concentration is observed as the bed width more increased to 21 cm in *Figure 3.5c*. As the spouting velocity increases, less averaged concentration got in the sampling regions more close to the bottom bed because higher velocity spreads the particles more upward and juts in the beginning of vortex formation and after descending vortexes, particles meet bottom bed regions. Still higher values of averaged concentration are observed in regions V and N.

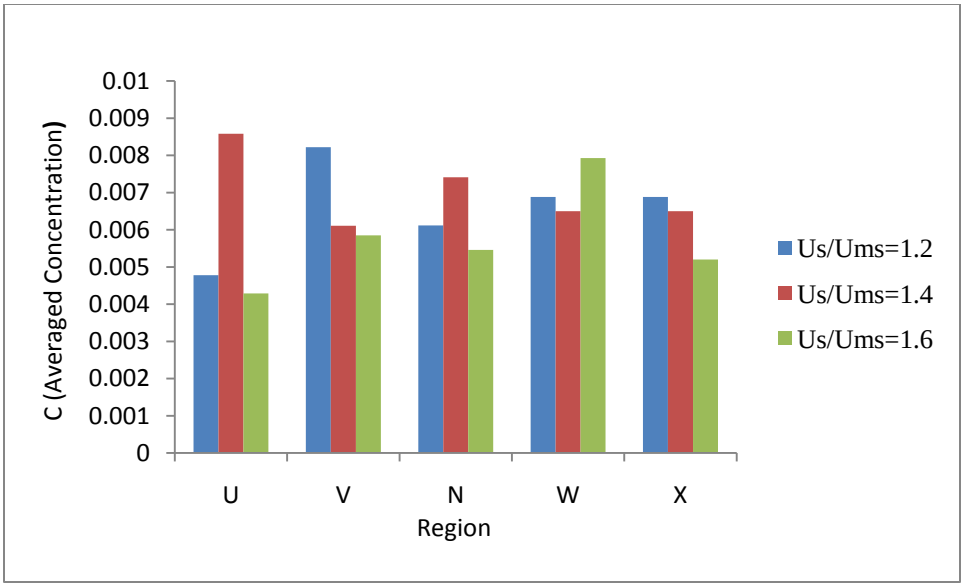

Figure 3.5b Radial distribution of tracer particles' concentration with various spouting gas velocities in spouted-bed with width of 15 cm

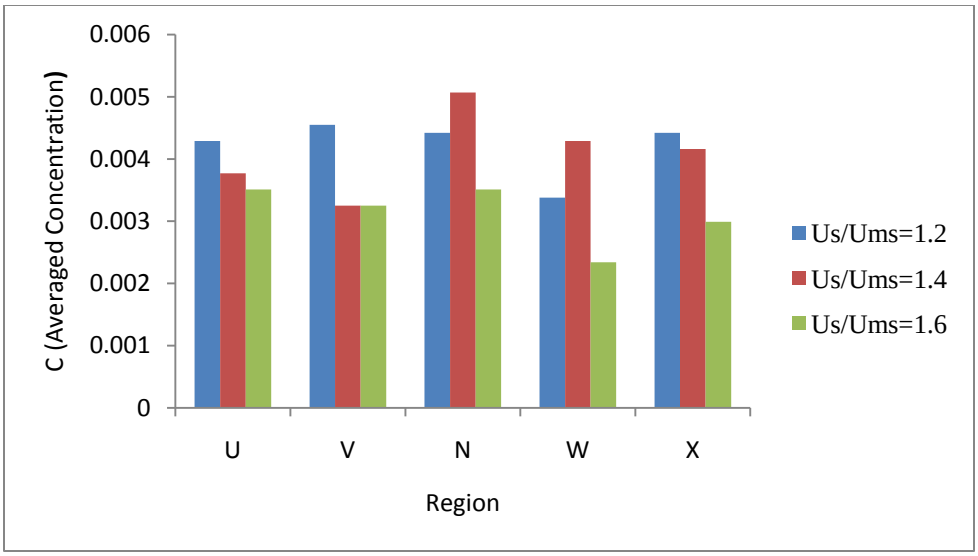

Figure 3.5c Radial distribution of tracer particles' concentration with various spouting gas velocities in spouted-bed with width of 21 cm

Due to the importance of understanding degree of mixing in both axial and radial direction and comparing qualitative results, *Figure 3.6a* shows M (mixing index) vs. U_s/U_{ms}. Five regions in axial and radial directions are representative for degree of mixing. Mixing index are calculated accordimng to equations (3.3) & (3.4). In 2D simulation of spouting gas velocities, highest degree of mixing index in radial direction is more than axial direction. It is valid for all spouting gas velocities examined and presented in *Figure 3.6a* for a spouted bed with width of 11 cm. Forces on the particles can describe the reason. Both have same declining trend of mixing index by increasing spouting gas velocity. Greater value of radial mixing could be discussed that in spout region, around the center axis where particles move upward with higher velocity, the drag force due to spouting gas velocity on particle is more than inherent gravity so braodly developes axial mixing and give uniform mixing. In *Figure 3.6a* both axial and radial mixing decreses with increasing spouting gas velocity. That indicated increasing gas velocity enhances particle mixing in this examined bed. Further incerasing bed width to 15 cm, gives mixing index diagram of *Figure 3.6b*. In *Figure 3.6b* instable mixing index is observed that the axial mixing is dominant on radial mixing in lower velocities and then axial and radial indexes catch a same value when U_s/U_{ms}=1.4 and then by increasing velocity radial mixing takes higher value than axial mixing index and gives uniformity to the axial mixing. Increasing bed width to 21 cm in *Figure 3.6c*, gives interesting feature that shows radial mixing has more values than axial mixing, this pattern indicates that axial mixing has more uniformity.

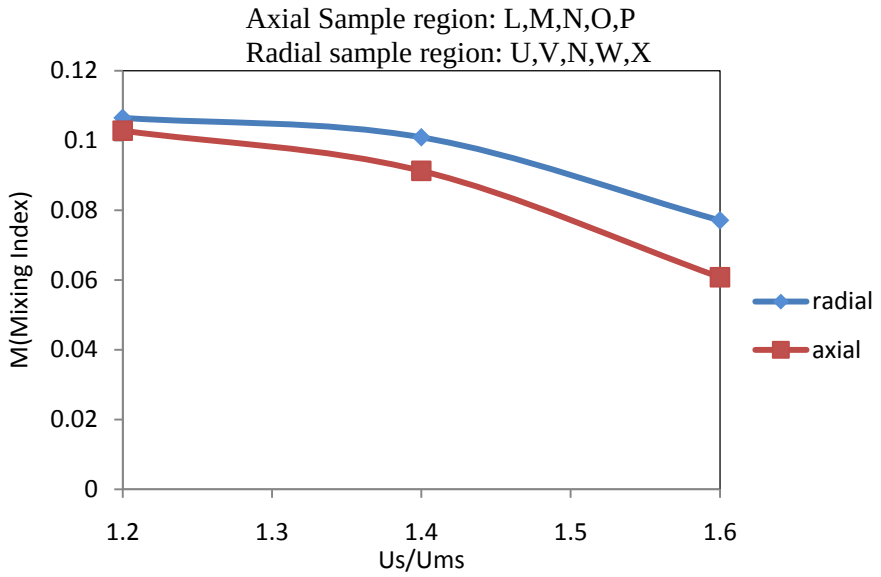

Figure 3.6a Mixing index in spouted-bed with width of 11 cm and various spouting gas velocities in radial and axial directions

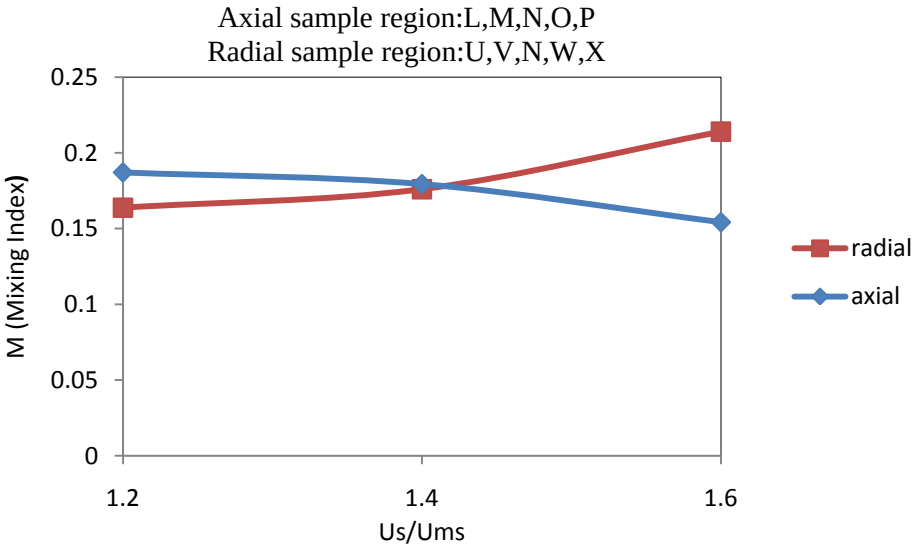

Figure 3.6b Mixing index in spouted-bed with width of 15 cm and various spouting gas velocities in radial and axial directions

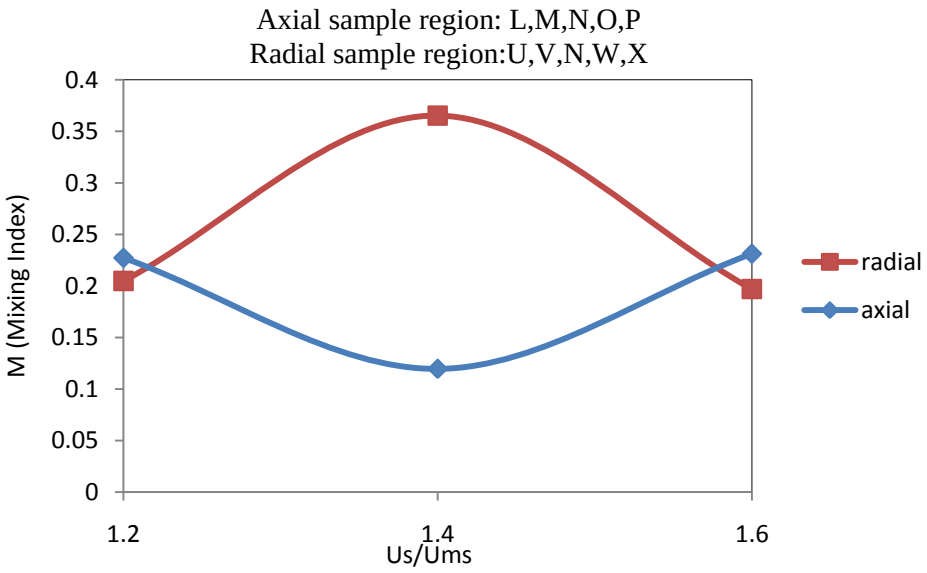

Figure 3.6c Mixing index in spouted-bed with width of 21 cm and various spouting gas velocities in radial and axial directions

3.2.3 Case 3: Effect of different fluidization velocities on tracer particles' distribution

Changing spouting gas velocity to the fluidizing gas velocity will change the void fraction and particles' velocity. Also, change of mixing pattern is expecting. So that, *Figure3.7a, 3.7b* and *3.7c* can show the results of axial distribution of particles' concentration in the same regions as *Figure 3.4a,3.4b* and *3.4c* used in given spouting gas velocity of U_s/U_{ms} = 1.1 and diverse fluidizing velocities. *Figure 3.7a* general pattern on concentration distribution of particles is that high concentration observed at the bottom of bed and decreases to the higher regions. This pattern is common in all examined fluidizing velocities. Totally, incresing fluidizing gas velocities, increases axial mixing. Comparing axial mixing due to the fluidizing velocities in *Figure 3.7a* shows greater values for particles' concentration in compare with axial mixing due to spouting gas velocity with the same bed in *Figure 3.4a*. This matter can aslo show the ability of MFIX software to model beds with fluidizing gas velocity conditions rather than spouting gas velocities. Higher values of tracers' concentration happens by increasing the fluidizing velocity.

Increasing bed width to 15 cm show less averaged concentartion of tracer particles in compare with smalerr bed due to the reason described for the same condition happens in spouting bed.

In *Figure 3.7b*, the concentration decreases as the particles reach higher regions of bed but increasing velocity enhances particles' concentration at the bed higher areas.

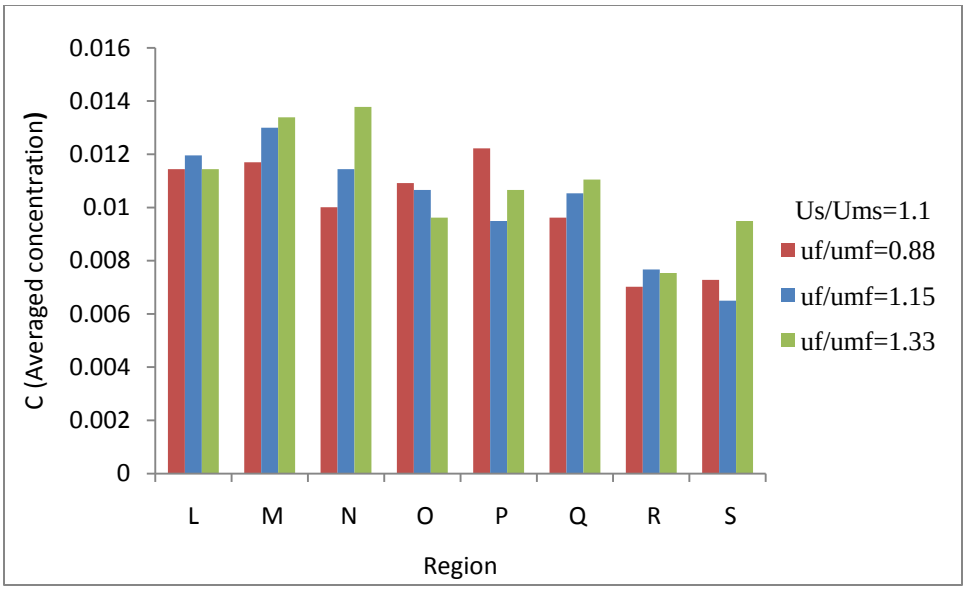

Figure 3.7a Axial tracer particles' concentration distribution in various fluidizing gas velocities in given spouting gas velocity of U_s/U_{ms} = 1.1 in a fluidized bed with width of 11cm

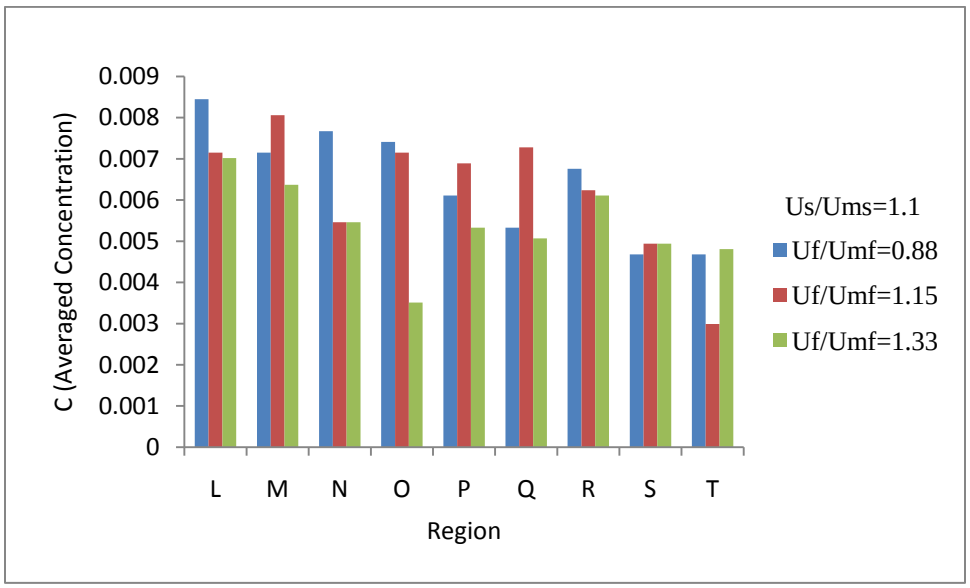

Figure 3.7b Axial tracer particles' concentration distribution in various fluidizing gas velocities in given spouting gas velocity of U_s/U_{ms} = 1.1 in a fluidized bed with width of 15cm

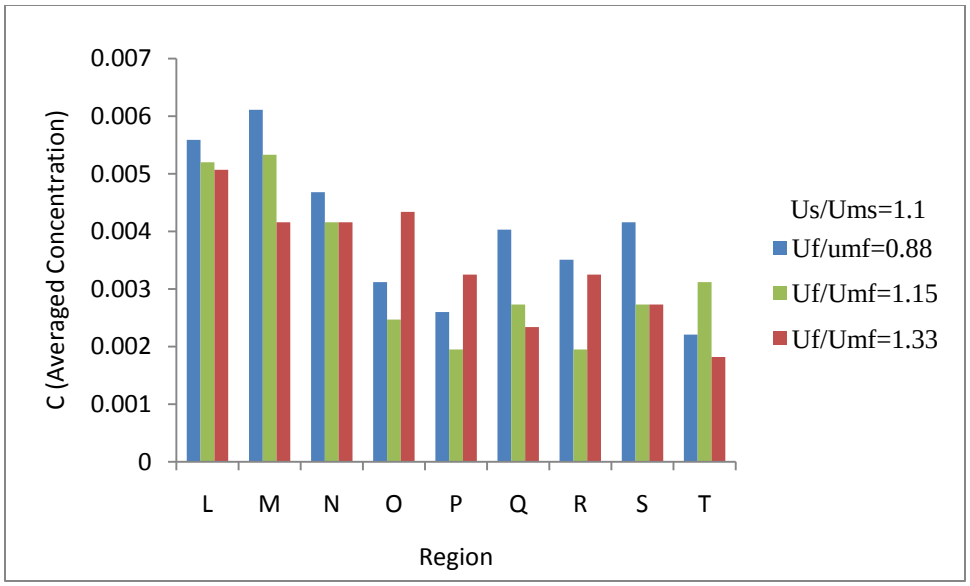

Figure 3.7c Axial tracer particles' concentration distribution in various fluidizing gas velocities in given spouting gas velocity of U_s/U_{ms} = 1.1 in a fluidized bed with width of 21cm

Figure 3.7c shows similar pattern of particles' distribution in bed. As discussed the higher value of averaged concentration is less than previous cases. As fluidizing velocity increases through the bed, concentration decreases in the lower parts of the bed and increase close to the fountain region.

Radial distribution with different fluidizing gas velocities is shown in *Figure 3.8a, 3.8b* and *3.8c*. In *Figure 3.8a*, by increasing fluidizing velocity, the averaged value of concentration increases in radial coordinate. Particles concentration spreads more uniform by increasing velocity when scattered from center of bed to the wall, in region V and N degree of concentration is considerable. Increase in fluidization velocity makes rapid tracer particles' movement and enhances higher diffusion of particles especially in annular area.
In *Figure 3.8b*, the bed width is increased to 15 cm and average concentration value decreases in compare with *Figure 3.8a*. In lower fluidizing velocity higher concentration is observed in the centerline as particles and this pattern does not change significantly by moving to the wall. Increasing in the fluidizing velocity has reverse effect on the radial movement in compare with *Figure 3.8a* and leads particles to have more concentration in the centerline and near wall. By increasing bed width to 21 cm in *Figure 3.8c*, this pattern improves that more averaged concentration is found in close to the centerline of the bed and as the sampling region location moves to the wall side, the concentration decreases. Increasing fluidizing velocity decreases the highest value of concentration in radial coordinate.

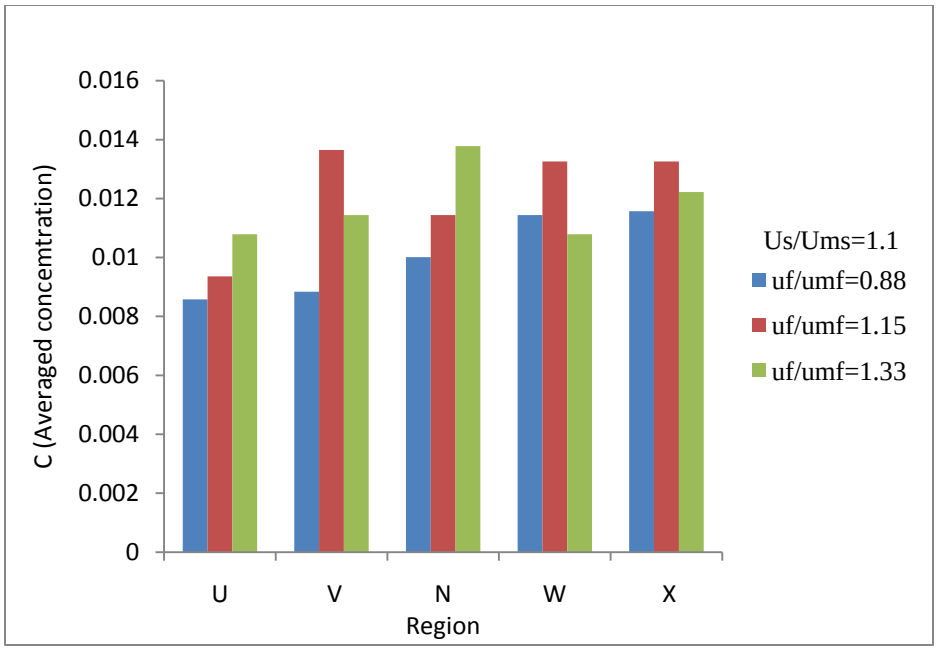

Figure 3.8a Radial distribution of tracer particles' concentration in various fluidizing gas velocities and given spouting velocity of U_s/U_{ms}=1.1, in fluidized bed with width of 11cm

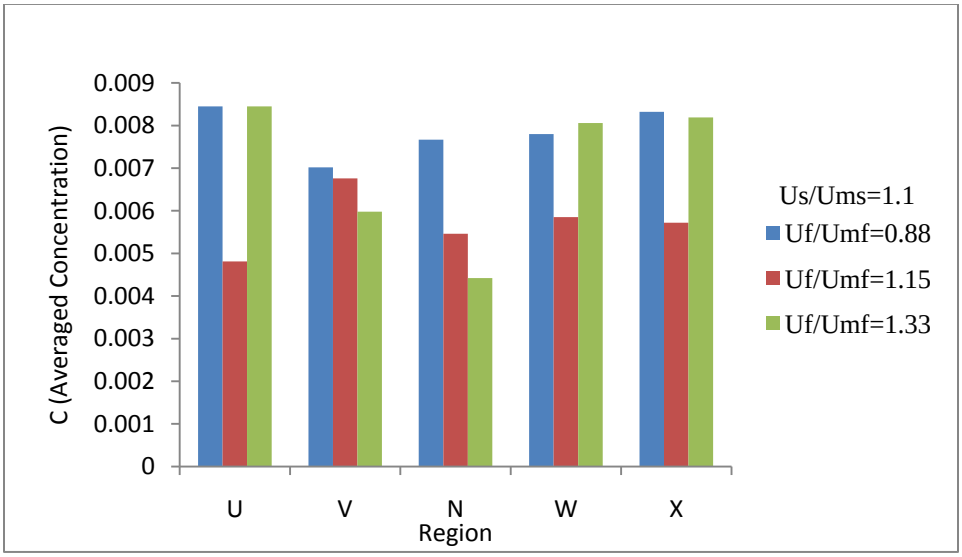

Figure 3.8b Radial distribution of tracer particles' concentration in various fluidizing gas velocities and given spouting velocity of U_s/U_{ms}=1.1, in fluidized bed with width of 15cm

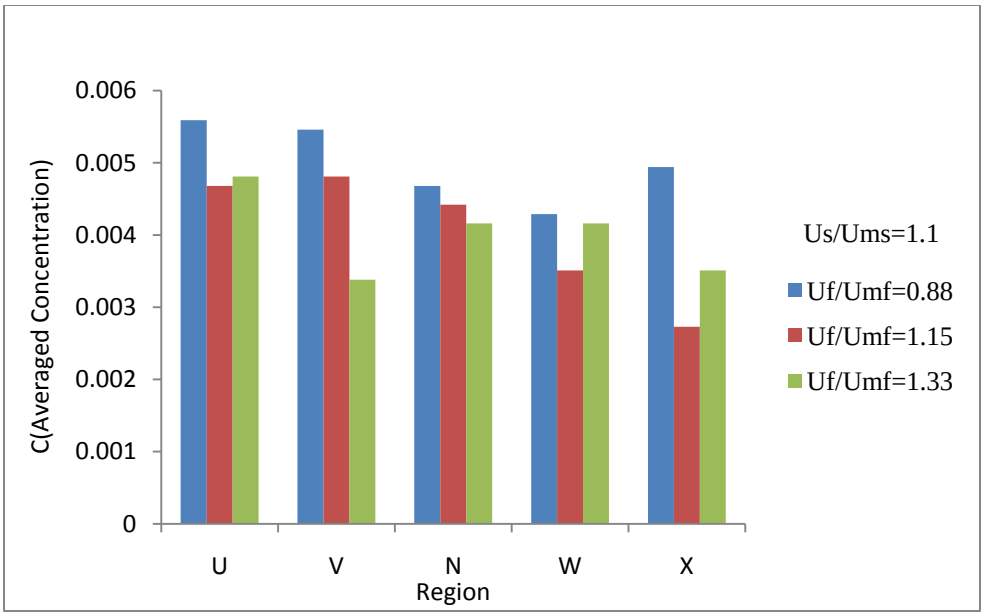

Figure 3.8c Radial distribution of tracer particles' concentration in various fluidizing gas velocities and given spouting velocity of U_s/U_{ms}=1.1, in fluidized bed with width of 21cm

As comparison between axial and radial mixing features is complicated, mixing index is considered as a factor that leads to better understanding of the mixing phenomena throughout the bed. Mixing index related to bed width of 11 cm in depicted in *Figure 3.9a*. Just like the cases which only spouting gas velocity was present in the bed(*Figure 3.6a*), in this bed radial mixing have higher value than axial mixing which indicates axial mixing gas advantage over radial mixing in bed with such condition in *Figure 3.9a* but the mixing index increases with increasing velocity. *Figure 3.9b*, is very similar to *Figure 3.6b* that uniformity is not observed in the bed. This bed with width of 15cm shows in lower fluidizing velocities, axial mixing is more dominant in the bed than radial mixing and this procedure reverses after radial and axial mixing meet the same value in the bed and afterward, the fluidizing velocity increases. *Figure 3.9c* shows bed mixing index with width of 21 cm; in contrast with results in *Figure 3.9a* and *3.9b*, axial mixing is dominant than radial mixing in the bed. It concluded that radial mixing is more uniform than axial mixing; moreover, fluidizing velocity increases radial movement in annulus area which helps reaching uniformity consequently. By increasing velocity, radial mixing in a small range gets higher value than axial mixing and makes axial mixing more uniform and favorable in the bed.

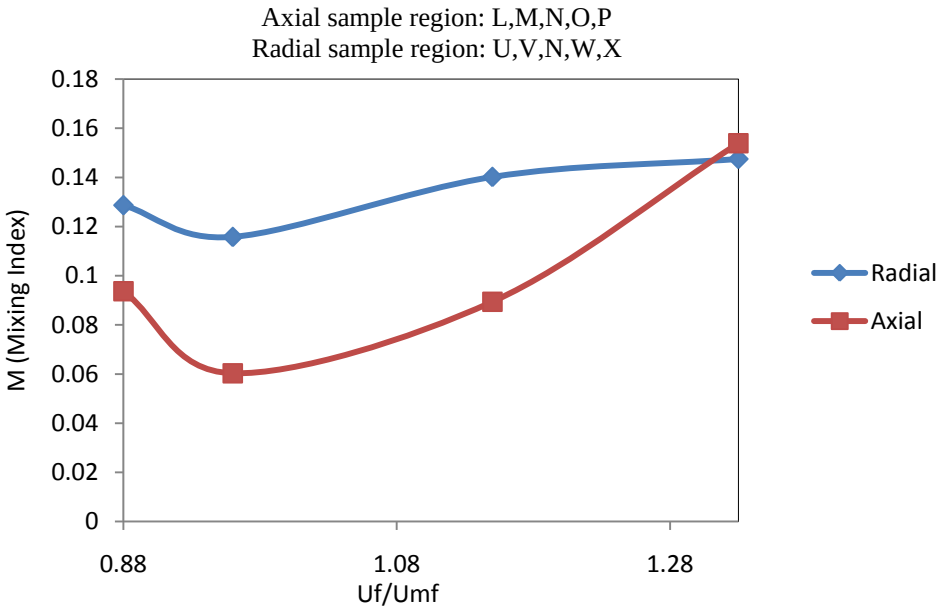

Figure 3.9a Mixing index at various fluidizing velocities and defined spouting gas velocity of U_s/U_{ms}=1.1, in fluidiezed bed with 11 cm width

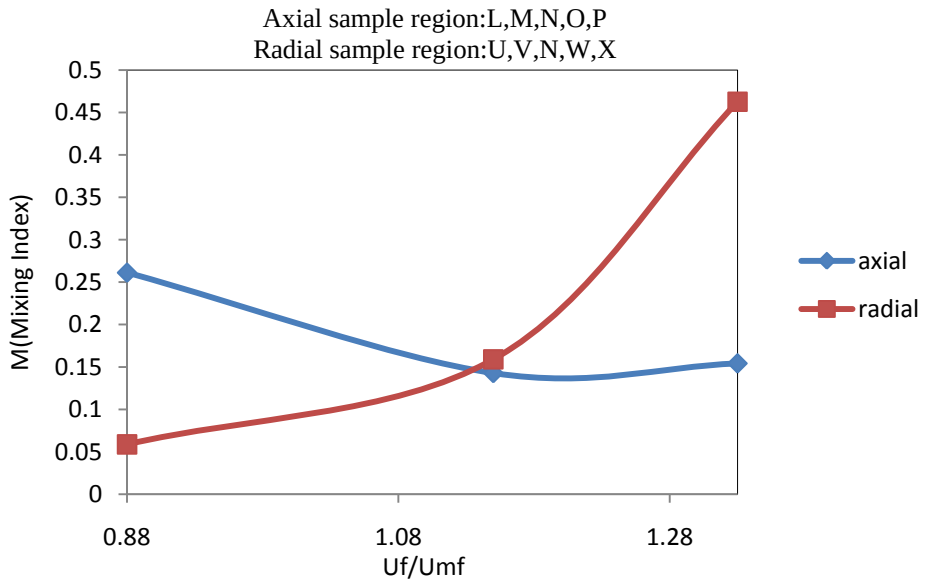

Figure 3.9b Mixing index at various fluidizing velocities and defined spouting gas velocity of U_s/U_{ms}=1.1, in fluidized bed with 15 cm width

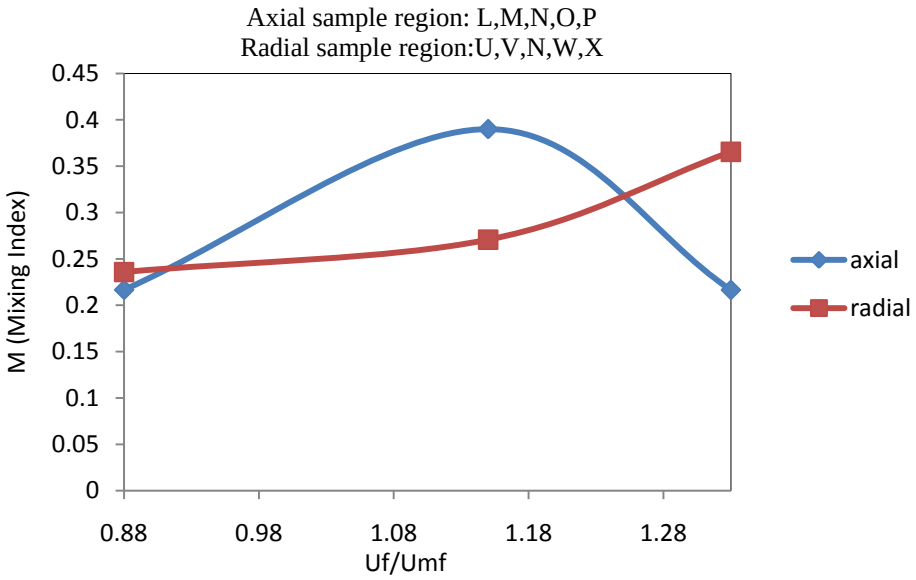

Figure 3.9c Mixing index at various fluidizing velocities and defined spouting gas velocity of U_s/U_{ms}=1.1, in fluidized bed with 21 cm width

3.3 General pattern-Influence of spouted gas velocity

3.3.1 Preferential position & velocity vectors

This part related to statistical investigation on effect of different spouting gas velocities and different bed dimensions on velocity vectors and preferential position of tracer particles, in two dimensional beds with various width of 11 cm, 15 cm, and 21 cm which number of total particles and tracer particles vary in each cases. In chapters, 3.3 and 3.4, a statistical analysis procedure is defined in MFIX to obtain results of preferential position; this statistical analysis method is described as follows:

1. The computational domain is discretized into quadrangular parts
2. Information of tracer particles stored
3. Number of times that particles move into each element is calculated
4. Particles mean velocity in each cell calculates

Table 3.2 shows number of total particles and tracer particles in each bed.

Table 3.2 Dimension of fluidized beds with relevant number of particles and tracer particles

Fluidized bed dimension (cm × cm)	Number of total particles	Number of tracer particles
11 ×100	1540	154
15×100	2100	210
21×100	2940	294

Bi-dispersed modeling with inert bed materials of $d_{p,inert} = 0.0028$ m and $\rho_{p.inert} = 900$ kg/m^3, with particles treated as tracers in mixing with $d_{p,inert} = 0.0028$ m, $\rho_{p.inert} = 905$ kg/m^3 are used.
This statistical analysis is done based on 50 seconds of bed performance.
Figure 3.10 illustrates preferential position of tracer particles in a bed with dimension of 11cm × 50 cm (10 cm bed material height). Effect of various spouting gas velocities of 1.2 U_{ms}, 1.4 U_{ms} and 1.6 U_{ms} is investigated.
Figure 3.10, *Figure 3.12* and *Figure 3.14*, show general distribution and tendency of tracer particles to move across regions of the beds during mixing time. Although tracer particles move all around the bed but the regions where particles most of the time move through, are in areas with highest value if normalized concentration and as goes from top to bottom of legend of normalized concentration with attention to the legend, and lowest value indicates, the probability of moving tracer particles to those regions decreases [33]. *Figure 3.10* shows effect of different spouting gas velocities on tracer particles' preferential position. To describe the general pattern, as velocity increases, the height of the bed increases and in lower velocity red spots at the bottom corner of the bed illustrates intention of tracer particles to move to these areas which the red

spots eliminate by increasing velocity and gives more uniform concentration of tracer particles in the bed and less preferred zone is observed.

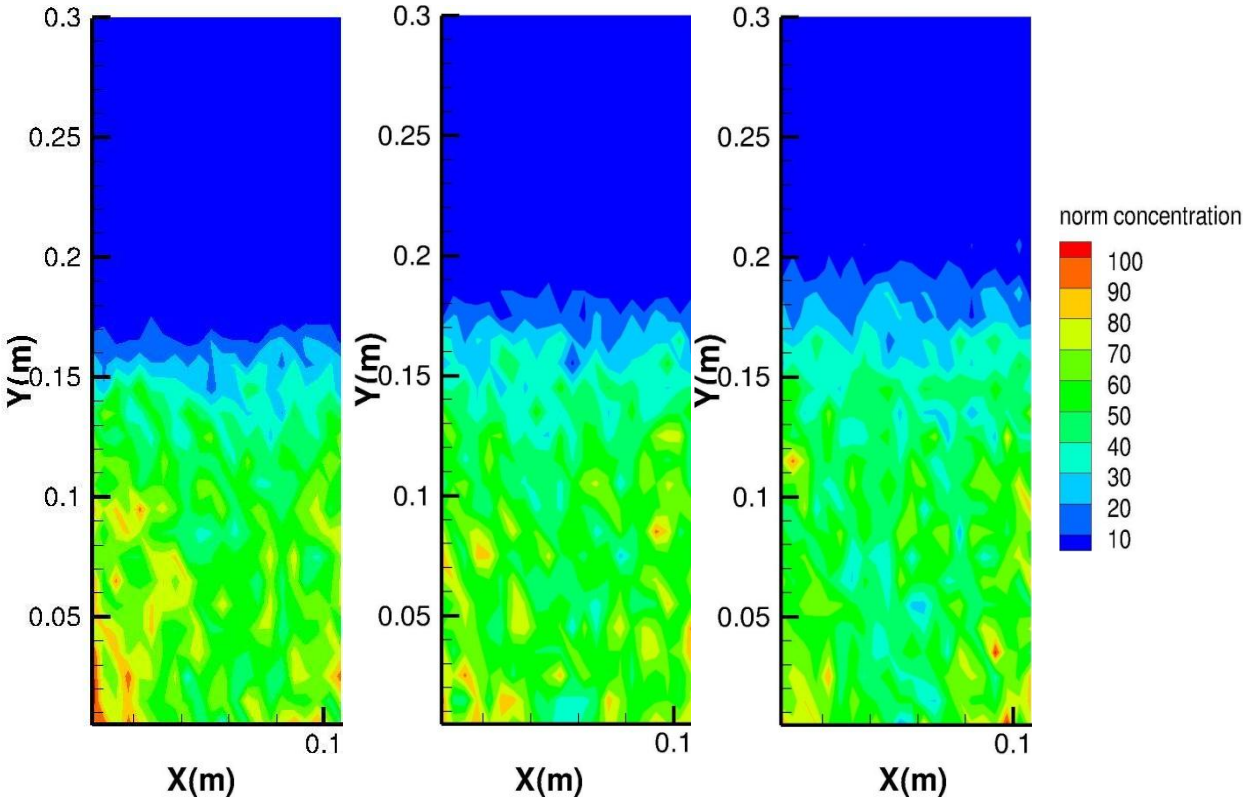

(a) U_s = 1.2 U_{ms} (b)U_s =1.4 U_{ms} (c)U_s = 1.6 U_{ms}

Figure 3.10 Effect of spouting gas velocity on preferential position of tracer particles in bed with width of 11 cm

In *Figure 3.10* the regions with less tracer particle concentration are more observant when the velocity increases in bed and ascending velocities of the tracer particles by matching with *Figure 3.11*. In *Figure 3.11(a)*, with the lowes velocity, one bubble path and two vortexes are indentified as vetrical channels and have lower tracer concentration and upward, higher velocities and velocity vector patterns also seen to have one main bubble path and two votexes as velocty incerase to *Figure 3.11(b)* and *(c).*

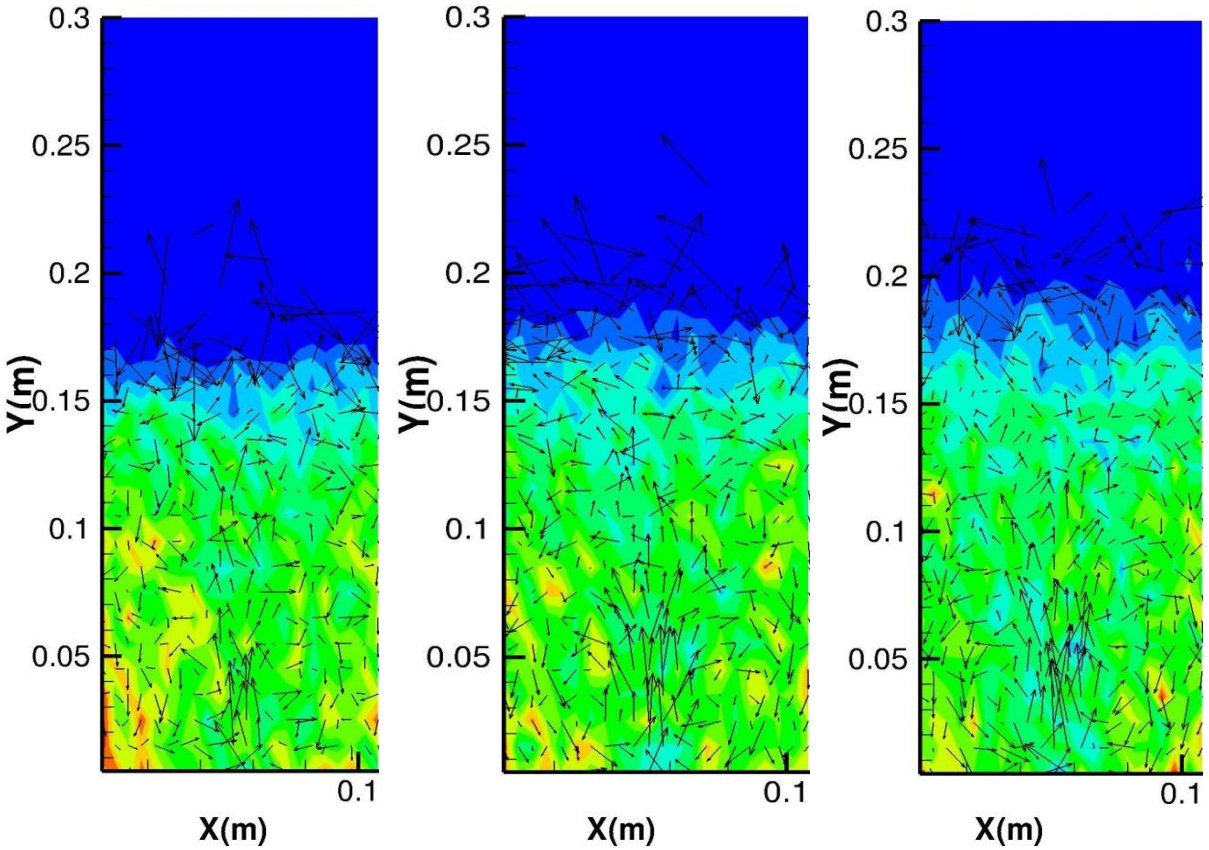

(a)U_s = 1.2 U_{ms} (b)U_s =1.4 U_{ms} (c)U_s = 1.6 U_{ms}

Figure 3.11 Velocity vector with increase in spouting gas velocity in fluidized bed with width of 11 cm

In *Figure 3.11(a),* highest concentration of fule particles is clear in rotational centerpoints in the created vortexes, which is close to the bottom bed surface. This pattern is eliminating as spouting gas velocity increases. In *Figure 3.11(c),* the regions with highest tracers concentration is suppressed and less major than *Figure 3.11(a).*

The same general pattern described for *Figure 3.9* and *3.10,* could be observed for *Figure 3.12, 3.13, 3.14* and *3.15*. In *Figure 3.12* and *3.14,* with increase in velocity the bed develops but comparing these two figures with *Figure 3.10,* dense bed gradually with increase the bed size and bed velocity eliminates. The flow regime shows dilute core and denser regions close to the walls, which is more sever in *Figure 3.14(c).* In the central part of this regime, solid and gas flow directed upward and make solid dense enough to throw the tracers upward, therefore the tracer region moves upward in the central region and moving downward in the denser region of the walls.

Increasing the bed width means increase in the total number of particles which is bed material included tracer particles.

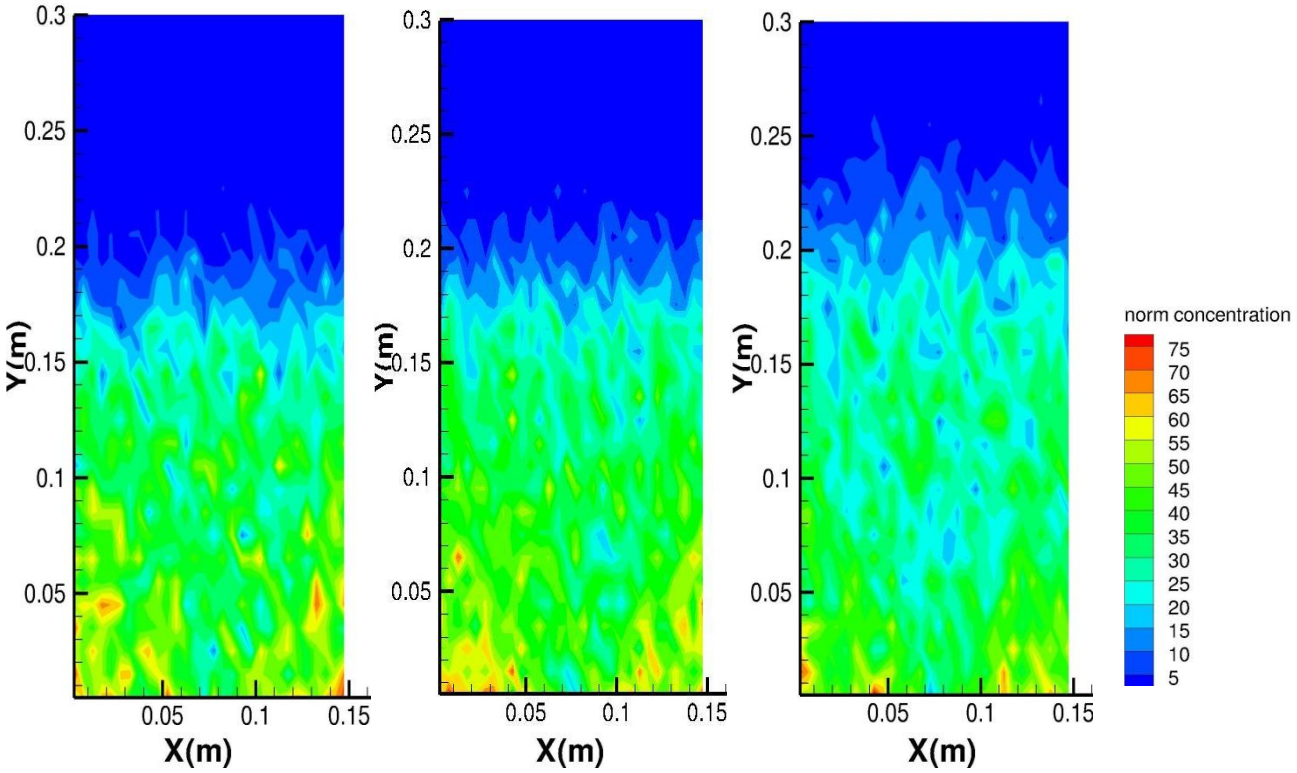

(a) U_s = 1.2 U_{ms} (b)U_s =1.4 U_{ms} (c) U_s = 1.6 U_{ms}

Figure 3.12 Effect of spouting gas velocity on preferential position of tracer particles in bed with width of 15 cm

In *Figure 3.11, Figure 3.13 Figure 3.15*,one main bubble path and two vortexes were created.It could conclude that number of vortexes and bubbles paths depend on amount of bed material and not to the fluidizing regime, in addition, the amount of bed material effects concentration and velocity field of tracer particles [34]. *Figure 3.12* and *Figure 3.14* shows that by increasing the bed width which in our cases means increasing amount of bed material consequently, the highest particle concentration value decreases. In *Figure 3.12(c),* and *Figure 3.14(c),* in compare with *Figure 3.10(c)* the core part of bed shows very low concentration of tracer particles in general and populates the tracers particles more at the bottom of the bed rather than central and upper parts.

Tracking *Figure 3.12* and *Figure 3.14*, individually, we notice that by increasing velocity, the tracer particles' concentration decrease in central and upper parts and more concentration is observed at the bottom bed, but the highest value of concentration decreases by increasing the velocity, these results are more severe in *Figure 3.14* with bigger width of bed of 21 cm and more bed inert materials. Also, considering *Figure 3.13* and *Figure 3.15*, individually, it is seen that in all the figures, one main bubble path and two vortexes are observable even in lower

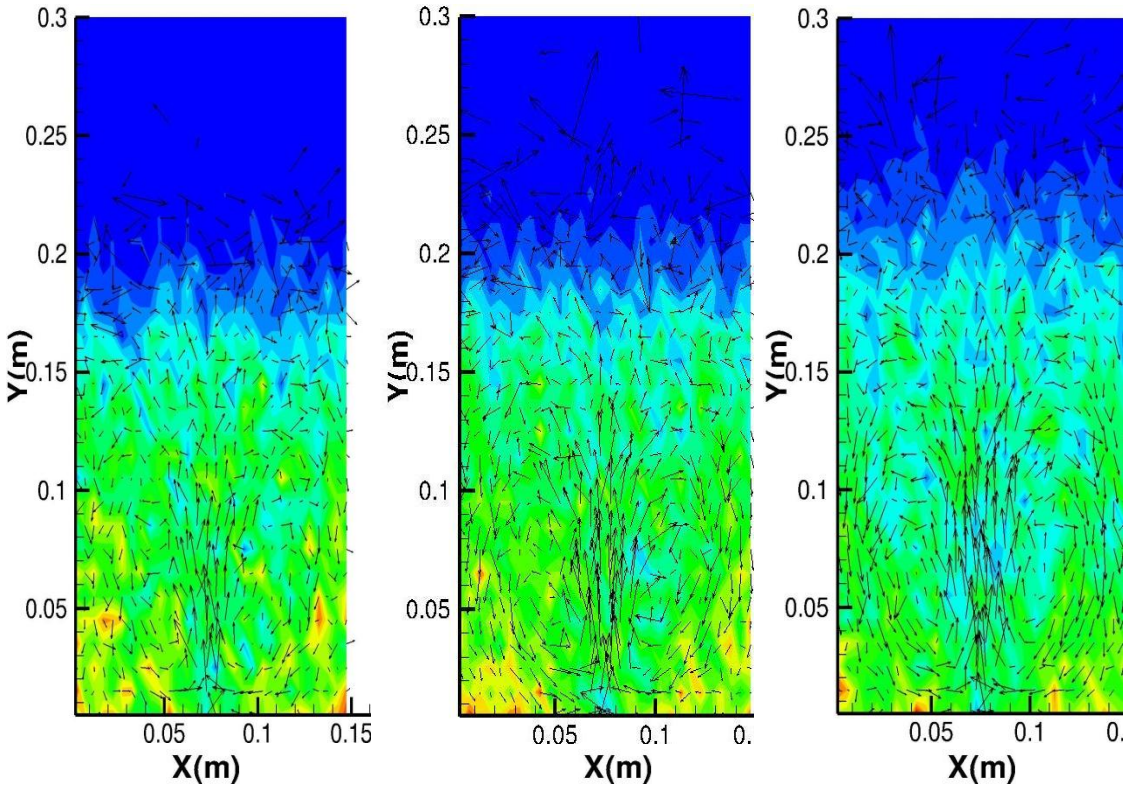

(a)U_s = 1.2 U_{ms} (b)U_s =1.4 U_{ms} (c)U_s = 1.6 U_{ms}

Figure 3.13 Velocity vector with increase in spouting gas velocity in fluidized bed with width of 15 cm

velocities and by increasing velocity, tracer particles enter a splash zone and spread up with higher velocity vectors. Again, these phenomena are more severe in *Figure 3.14* and very strong mixing with highest velocity vectors happen in a bigger bed with width of 21 cm and U_s/U_{ms}= 1.6.

In *Figure 3.14* the concentration of tracer particles has higher value at the bottom of the bed, indicates that the tracer particles have more tendency to pass through this area and may segregate.

Increasing in bed inert material leads to increase in velocity of tracer particles. Comparison in *Figure 3.11* with *Figure 3.13* and *3.15* even if in *(a)* cases in each figure, we conclude that velocity fields has higher value in bigger beds and even in same velocities in each case, the velocity fields in bigger beds, distributes in higher regions in the bed (note the change in scales).

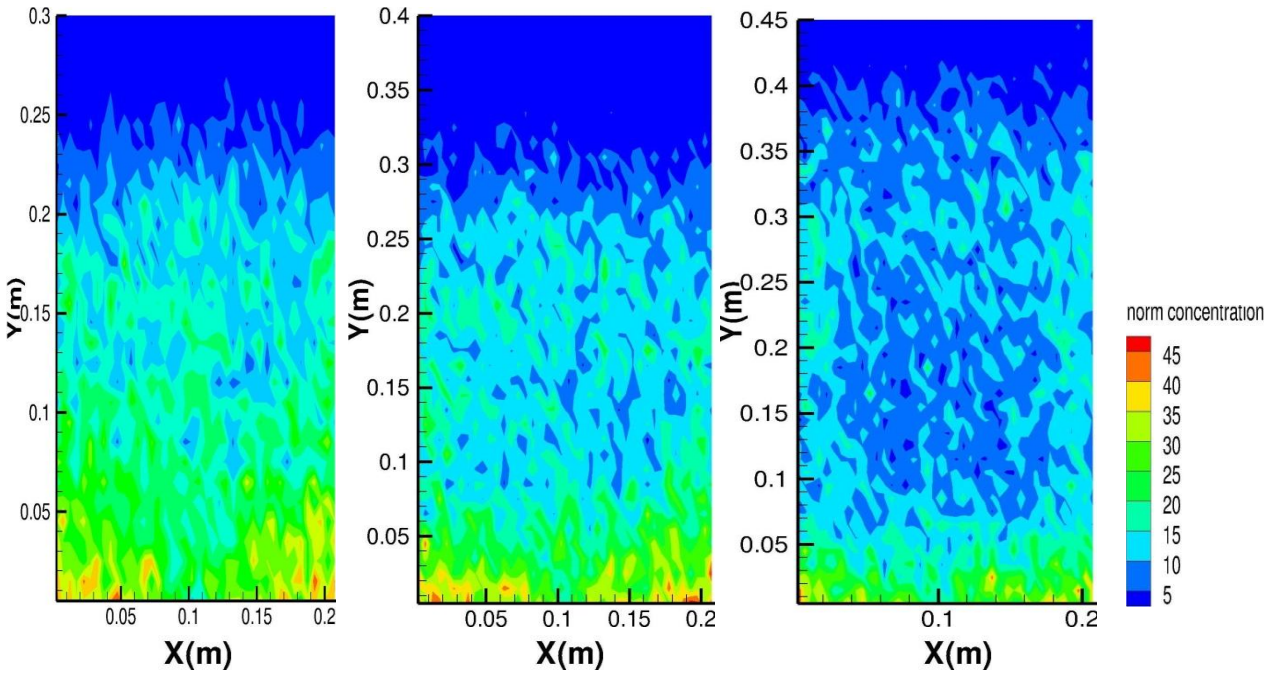

(a)U_s = 1.2 U_{ms} (b)U_s =1.4 U_{ms} (c)U_s = 1.6 U_{ms}

Figure 3.14 Effect of spouting gas velocity on preferential position of tracer particles in bed with width of 21 cm

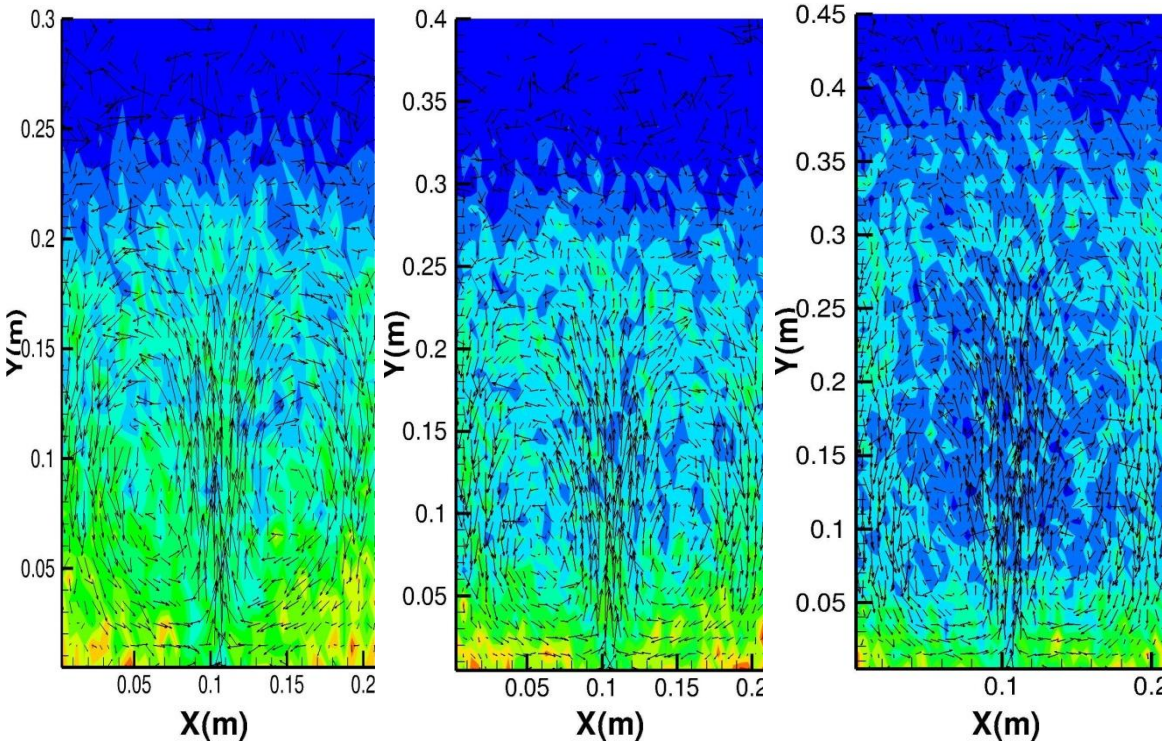

(a) U_s = 1.2 U_{ms} (b)U_s =1.4 U_{ms} (c)U_s = 1.6 U_{ms}

Figure 3.15 Velocity vector with increase in spouting gas velocity in fluidized bed with width of 21 cm

3.3.2 Horizontal Dispersion

Mixing of particles plays a great role in the performance of spouted and fluidized beds. Gas-solid mixing in beds caused by different mechanisms; such as, global mixing and local mixing of particles. The former causes due to the net circulation of solids in the bed because of gas-bubbles rising up and bring the solids to the surface; bubbles burst and disperse the particles then descent to the bottom of the bed in form of emulsion, this mechanism called bubble-induced mixing which is illustrated by the bubbles' movement. Parallel to the global mixing, local mixing of solids happen when the bubbles rise and between emulsion. This mixing is characterized by the random movement of solid particles. Both the mechanisms could be described by Fick's law within diffusion with different diffusion coefficients know as dispersion coefficient for the global mixing and particle diffusivity for the local mixing [34]. Local mixing and particle diffusivity described by Brownian movement, wall interaction and appraised by the random walk theory based on Lagrangian coordinates on set of particles [35-37].
Johansson et al. (2006) suggested a method to calculate local dispersion coefficient through experimental work. They implemented equation (3.7) to calculate local solid dispersion coefficient, as [34]:

$$D_{k,n} = \frac{\Delta l_{k,n}^2}{2.\Delta t_n} \tag{3.7}$$

With $k=x, y$ and for $n= 1,..., N$.
Δt_n is calculated based on the shutter time of the video camera which is stated generally in order of 10^{-2} seconds or lower. And $\Delta l_{k,n}$ is the change of displacement from one video frame to another. High values of Δt_n increase the risk of underestimation of dispersion coefficient [34].

Figure 3.16 shows horizontal dispersion for bed with width of 11 cm. *Figure 3.16(b)* and *3.16(c)* are similar in respect of general pattern of local dispersion and the lowest and highest value for dispersion in the bed. Highest value of dispersion should match with areas where bubbles burst. *Figure 3.16(a),* showed one main bubble paths and two vortexes, the highest dispersion value in the middle of this picture and some spots in the surface of the bed is observable. Bubbles lead the particles to the surface and when burst and erupt, spread the particles around and make the locations when maximum of horizontal dispersion happens.
In *Figure 3.16*, the more noticeable dispersion locations are close to the sidewalls, where then particles were pushed to the middle of the bed which is the region where one main path are recognized and have less dispersion and more concentration of particles. Increasing the spouting gas velocity in *Figure 3.16*, approves a great effect of velocity on horizontal dispersion that make more uniform bed in this aspect and change the highest value of horizontal dispersion from *Figure 3.16(a)* to *(b)* and *(c).*

The pattern of horizontal dispersion which described for *Figure 3.16* is observable in *Figure 3.17*, with increase in value of horizontal dispersion. It indicates that by increasing bed material even in the same velocity, the horizontal dispersion increases extensively.
Particles are more uniformly spread in the bed in *Figure 3.17(a)*, *(b)* and *(c).* Moreover, as the velocity increases, the height of bed basically increases. Still the regions with maximum amount of dispersion are close to sidewalls, where the vortexes and particles descend and circulate to form the new vortex in the bed.
Figure 3.18 is a bed with width of 21 cm that the bed material is more than the last case. Generally, the highest value of dispersion is more increases in compare with cases in *Figures 3.16* and *Figure 3.17*. Notice to the change of scale shows that dispersion happens in higher regions in the bed. The pattern for horizontal dispersion considered close to the feature to the previous cases that more value of horizontal dispersion is observable in the sidewalls where the vortexes and particles descend. Special pattern is observed when velocity increases; more formation of bubbles happen in *Figure 3.18(b)* and *(c)* so the vortexes rise and speed up more than other cases and move particles upward then spread more to the sidewalls as seen in *Figure 3.18(c)* severely. Note that value of horizontal dispersion is much more than other cases.
To conclude, by increasing the amount of bed material, dispersion coefficient value increases generally and severely along the sidewalls. Along center of the bed where the vortexes move upward and share a path together, horizontal dispersion is noticeable. By increasing the velocity, horizontal dispersion increases.

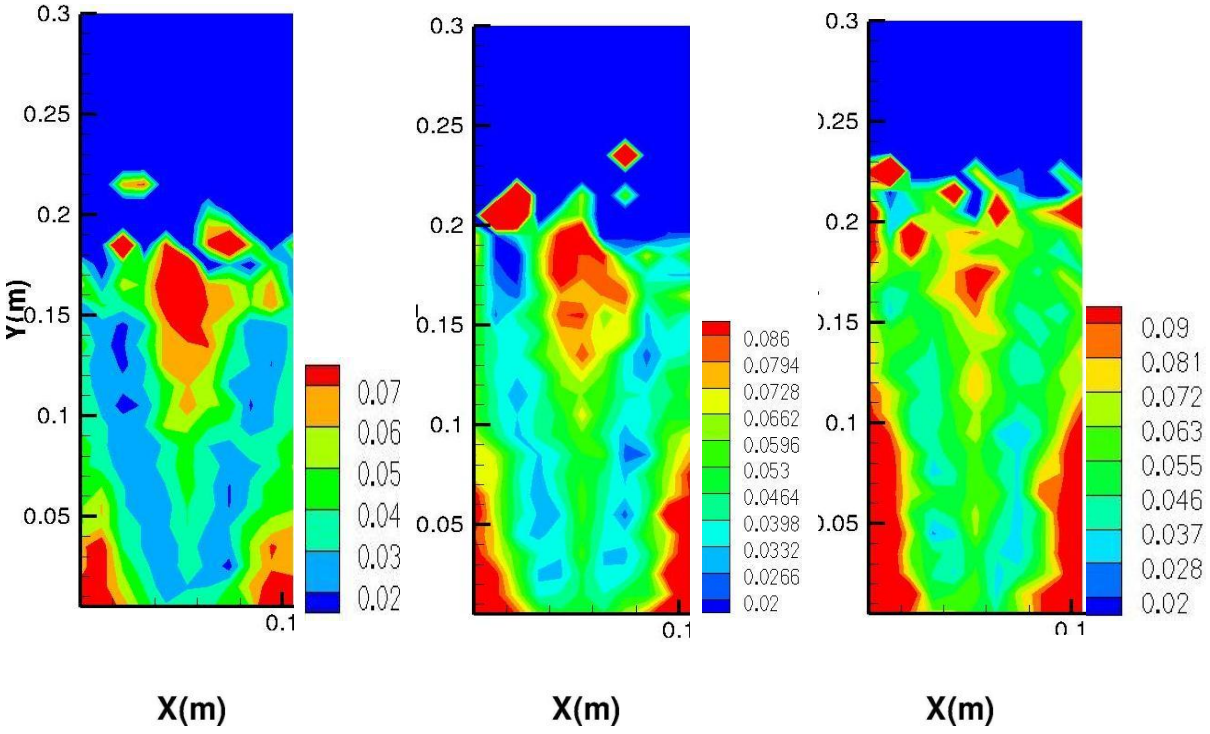

(a)U_s = 1.2 U_{ms} (b) U_s =1.4 U_{ms} (c)U_s = 1.6 U_{ms}

Figure 3.16 Horizontal dispersion with increase in spouting gas velocity in fluidized bed with width of 11 cm

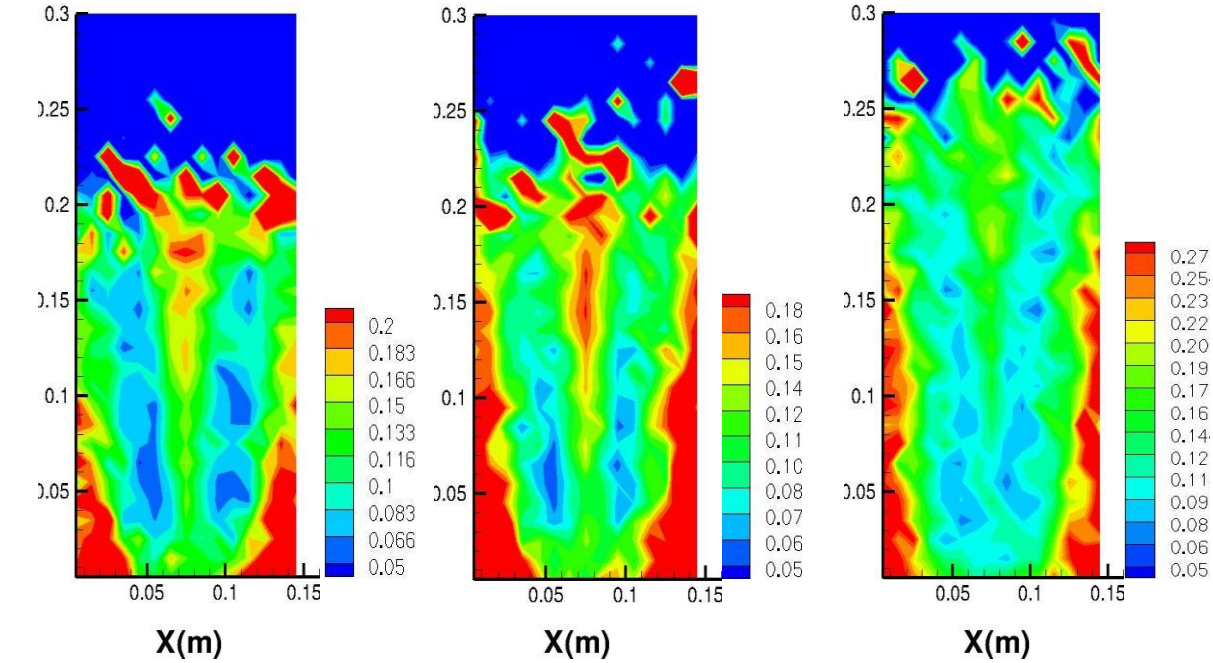

(a)U_s = 1.2 U_{ms} (b)U_s =1.4 U_{ms} (c)U_s = 1.6 U_{ms}

Figure 3.17 Horizontal dispersion with increase in spouting gas velocity in fluidized bed with width of 15 cm

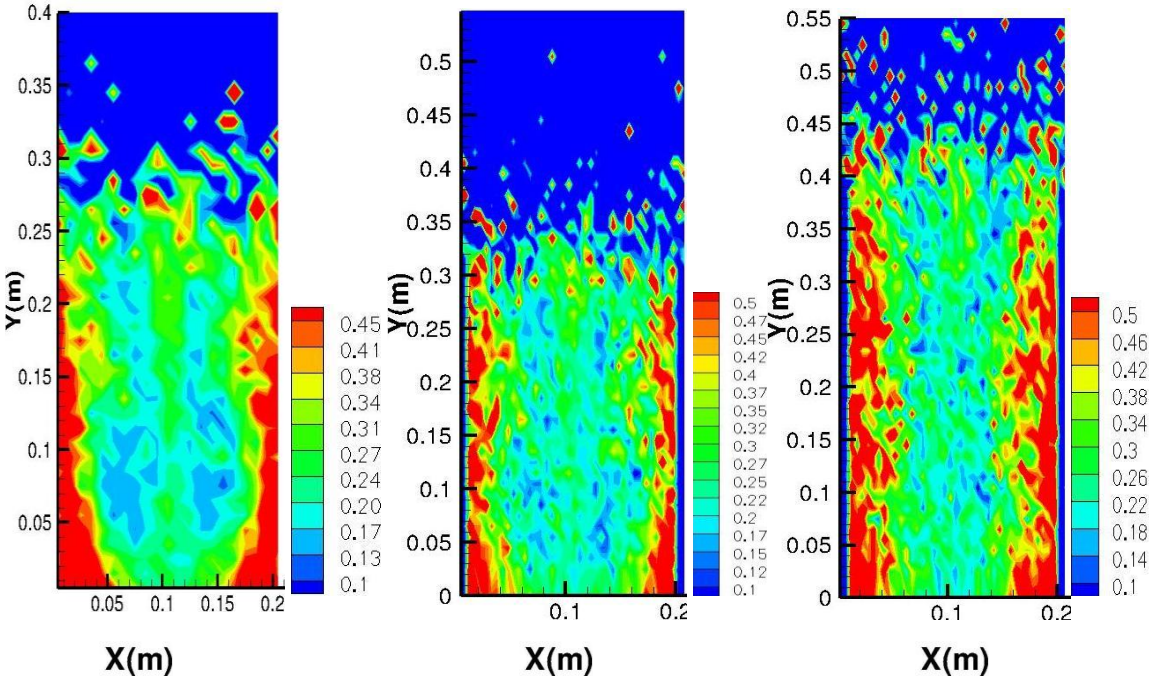

(a)U_s = 1.2 U_{ms} (b)U_s =1.4 U_{ms} (c)U_s = 1.6 U_{ms}

Figure 3.18 Horizontal dispersion with increase in spouting gas velocity in fluidized bed with width of 21 cm

3.4 General pattern- Influence of fluidizing gas velocity

3.4.1 Preferential position and velocity vectors

Preferential position in *Figure 3.19* shows the tendency of tracer particles to move more across those areas during circulation. In *Figure 3.19(a), (b)* and *(c)* the highest value of tracers' concentration are observed in close to the bottom bed and sidewalls, which decreases with increasing velocity; these areas are parts which vortexes descend and particles settle down to start a new circulation of vortex. More uniform concentration of particles is appeared in bed with increasing velocity. In *Figure 3.21*, this pattern is distinguished but the highest value of normalized concentration decreases; in *Figure 3.21(a),* highest value of concentration is observable at the bottom of the bed and by increasing the velocity this pattern changes and distribution of tracer particles shape more uniform in the bed with less value of concentration. Increasing the bed width to 21 cm in *Figure 3.23*, shows more change in the tracer particles change of pattern that in *Figure 3.23(a)* like *Figure 3.19(a)* and *Figure 3.21(a)* highest value of concentration is seen that these areas eliminates gradually by increasing velocity. But with increasing the bed material and bed dimension, more bubbles rise upward and burst so it changes the circulation of tracer particles in bed; careful look at the *Figure 3.23* shows the regions where tracer particles have less attended are more observable and these regions show where bubbles are present. In conclusion, by increasing the bed material, more bubbles form in even same velocities with increasing velocity, more uniform pattern of tracer particles' distribution is observed and consequently, the bed height has increased considerably, but the highest value of concentration decreases.

Considering velocity vectors which show bubbles formation in the bed that move particles upward and then descending particles with ending up the vortexes circulation; in *Figure 3.20,* four vortexes with two main paths is seen and by increasing velocity it gets clear shape to the one mail bubble path and two vortexes. In *Figure 3.22* this pattern improves even in lower velocities and it shows by increasing the bed materials we can improve the velocity vector pattern in the bed and better mixing happen. By increasing velocity better mixing of tracer particles in bed is observable through two vortexes and one main path for bubble eruption and dispersing tracer particles to the wall side then particles move down with ending up the vortexes and segregate at the bottom bed to start new circulation of vortex. Increasing more the bed material with bed width of 21 cm in *Figure 3.24* clears out more the effect of amount of bed material on the formation of bubbles, expansion and eruption of bubbles that simultaneously moves up particles and causes better mixing in the bed. Even in lower velocities, a clear main path and two vortexes are observable while increasing fluidizing velocity gradually gives more uniform and clear cut of vortexes that in different heights throw the tracer particles up and develop the mixing.

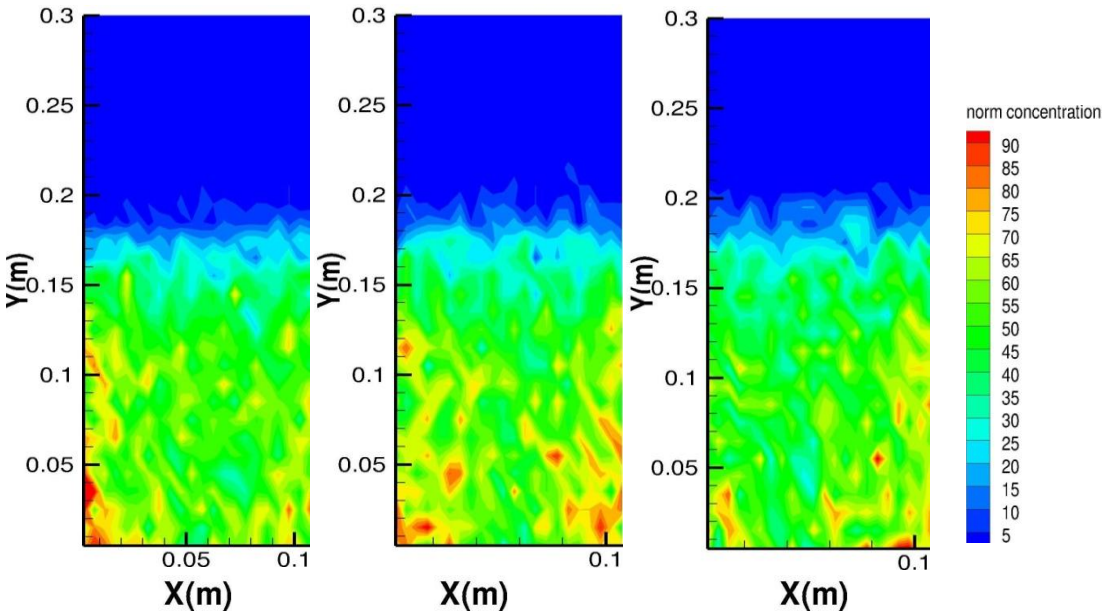

(a)U_f = 0.88 U_{mf} (b)U_f =1.15 U_{mf} (c)U_f = 1.33 U_{mf}

Figure 3.19 Effect of fluidization velocity with constant U_s/U_{ms} =1.1 on preferential position of tracer particles in bed with width of 11 cm

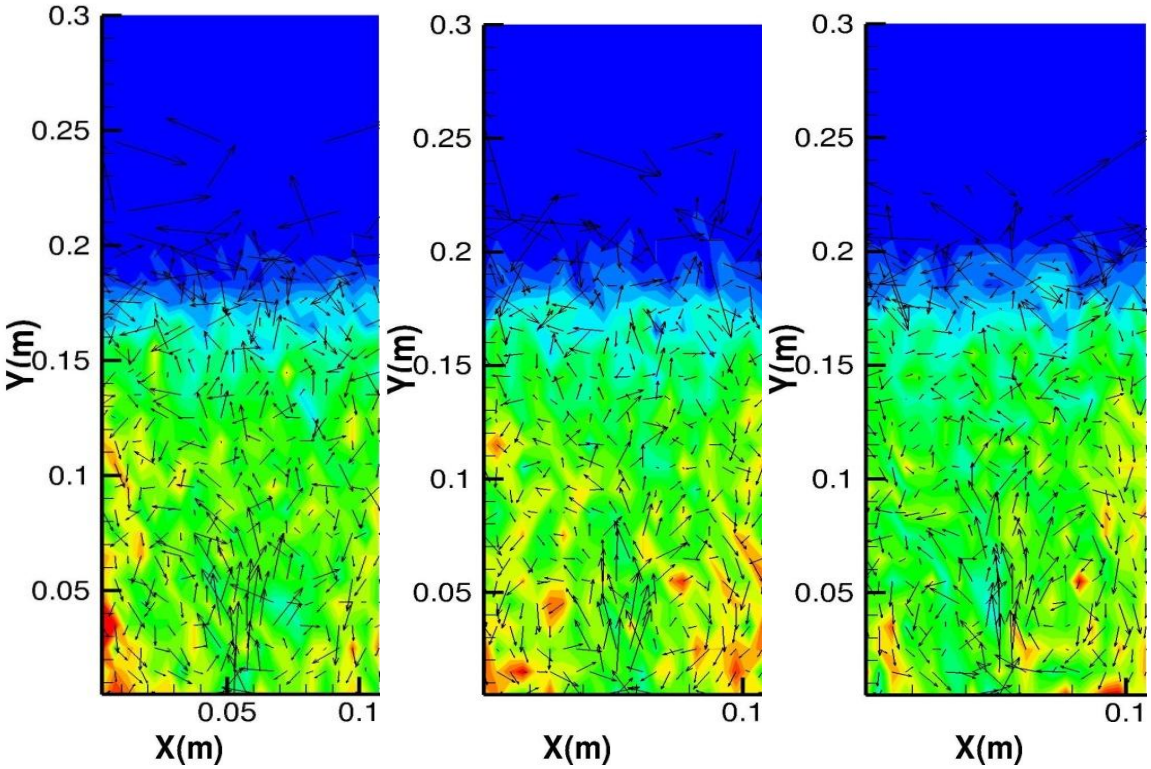

(a)U_f = 0.88 U_{mf} (b)U_f =1.15 U_{mf} (c)U_f = 1.33 U_{mf}

Figure 3.20 Effect of fluidization velocity with constant U_s/U_{ms} =1.1 on velocity vector of tracer particles in bed with width of 11 cm

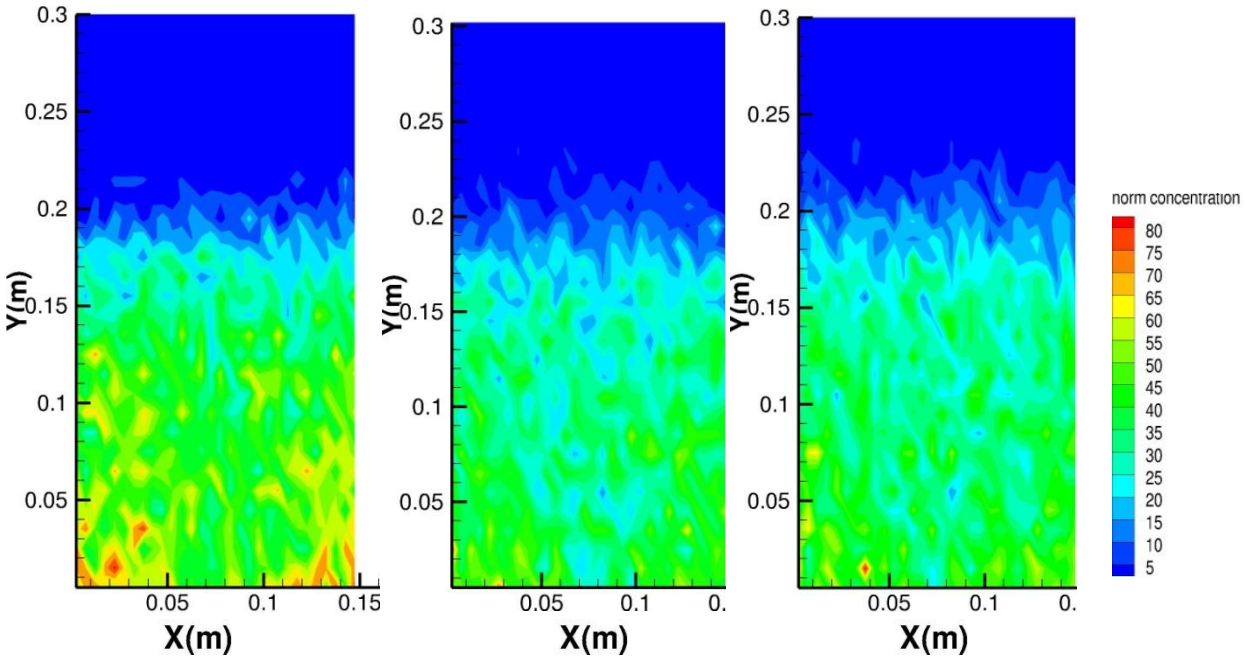

(a)U_f = 0.88 U_{mf} (b)U_f =1.15 U_{mf} (c)U_f = 1.33 U_{mf}

Figure 3.21 Effect of fluidization velocity with constant U_s/U_{ms} =1.1 on preferential position of tracer particles in bed with width of 15 cm

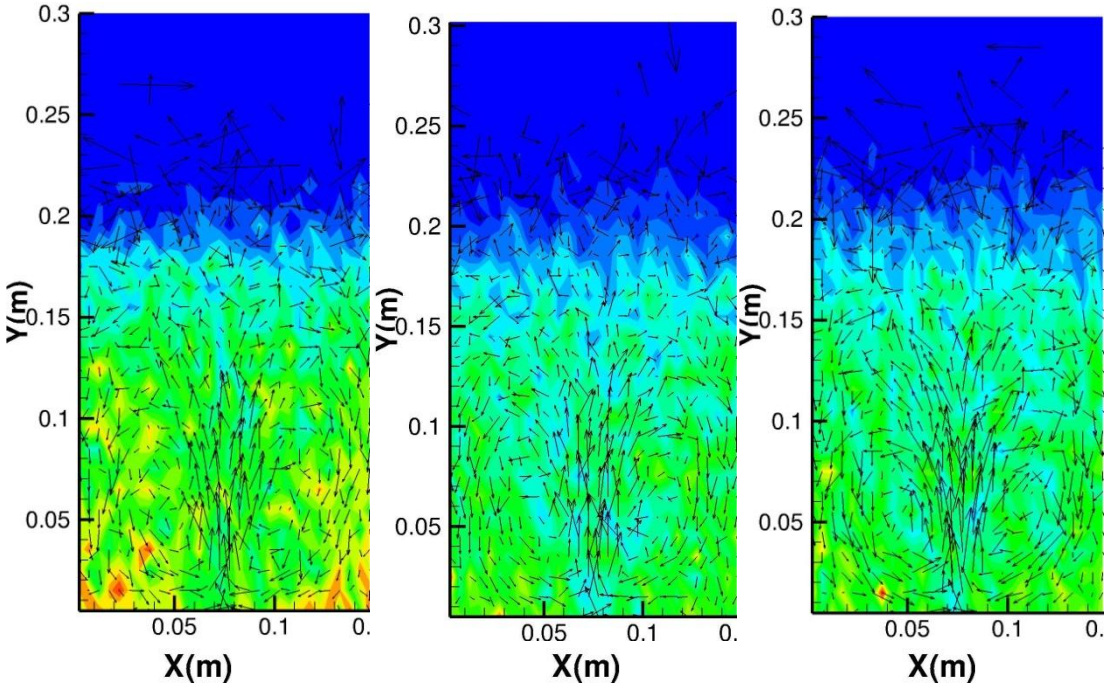

(a)U_f = 0.88 U_{mf} (b)U_f =1.15 U_{mf} (c)U_f = 1.33 U_{mf}

Figure 3.22 Effect of fluidization velocity with constant U_s/U_{ms} =1.1 on velocity vector of tracer particles in bed with width of 15 cm

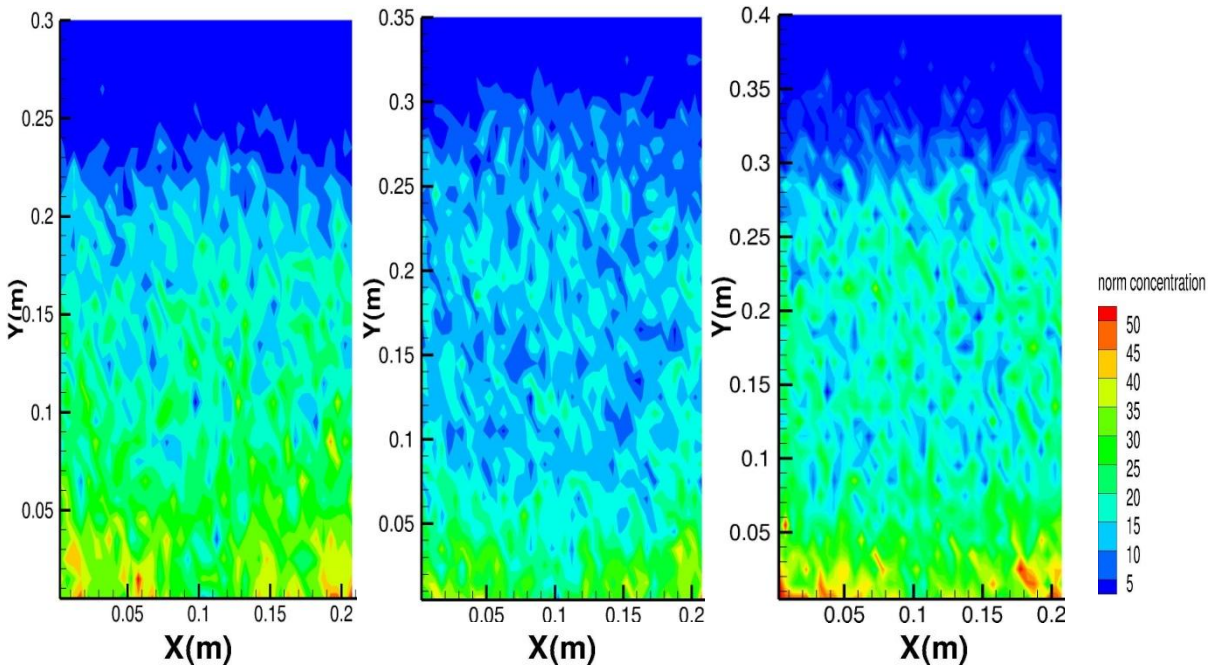

(a)U_f = 0.88 U_{mf} (b)U_f =1.15 U_{mf} (c)U_f = 1.33 U_{mf}

Figure 3.23 Effect of fluidization velocity with constant U_s/U_{ms} =1.1 on preferential position of tracer particles in bed with width of 21 cm

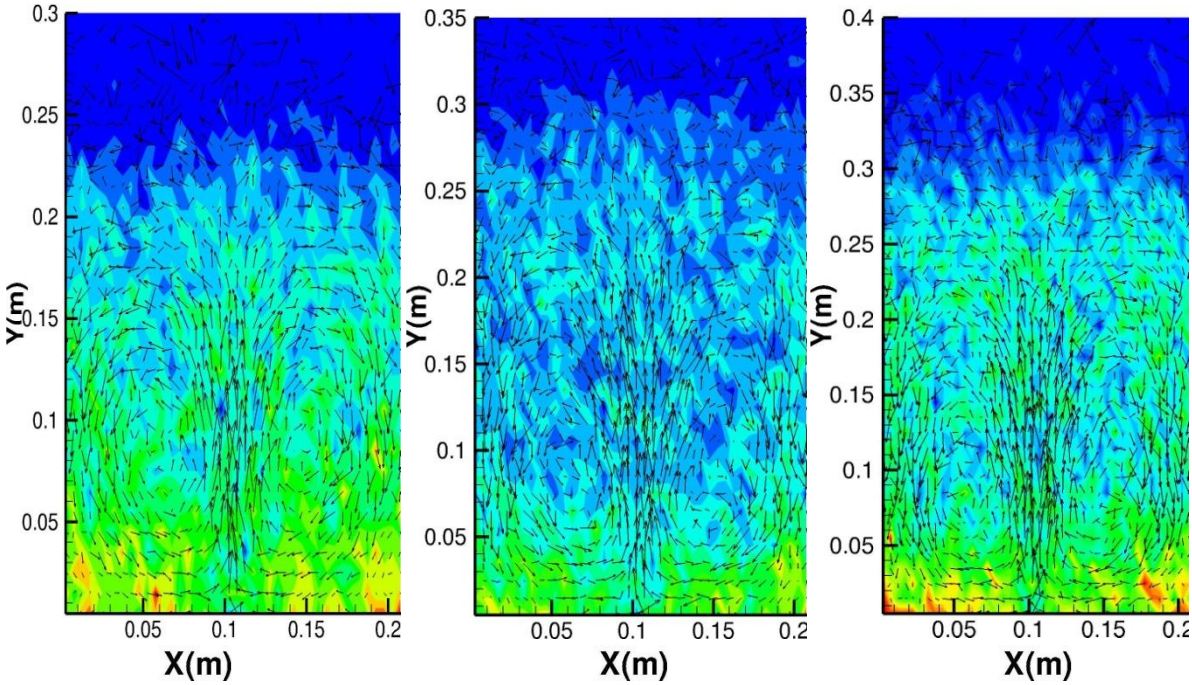

(a)U_f = 0.88 U_{mf} (b)U_f =1.15 U_{mf} (c)U_f = 1.33 U_{mf}

Figure 3.24 Effect of fluidization velocity with constant U_s/U_{ms} =1.1 on velocity vector of tracer particles in bed with width of 21 cm

Comparing preferential position features and velocity vectors in figures with just spouting gas velocity and the others with presence of fluidizing velocity does not show large difference and the general pattern remains same in both cases, which may indicate that the most important parameter is bed material and superficial velocity of gas that spreads through the bed.

3.4.2 Horizontal Dispersion:

Horizontal disperision as discussed before via the formulas suggested in litreature, indicates the tendency of particles to spread horizontally in the specific areas of the bed. In *Figure 3.25*, at lower fluidizing velocity, higher horizontal dispersion happens all along the wall. And less dispersion along the center line of the bed; by increasing fluidizing velocity, a "v" path appears and shows horizontal dispersion at the bottom corners and to some extend on the bed surface where vortexes descend and start to fall down. The dispersion regions are noticeably decreases with increasing fluidizing velocity in bed with width of 11 cm but the highest value of horizontal disperion increases gradually. In *Figure 3.25(a)* this pattern remains as more horzontal dispersion is observed in the surface and close to the walls at bottom bed. By increasing velocity, highest value for horizontal dispersion decreases. And gradually increasing the fluidizing velocity in *Figure 3.25*, shows increase in the regions of bed where tracers intend to disperse horizontally through the same pattern that close to the walls and in the center line tracer particles intend to disperse more. Increasing bed material to the bed with width of 21 cm shows increase in horizontal dispersion while particles gather more at the centerline of the bed and make less values of horizontal dispersion along the center line and more values of dispersion are observable at the wall sides, bottom bed and surface of the bed.

This structure remains by increasing fluidizing velocity. Average value for horizontal dispersion increases but the large region assigned to less value of dispersion in *Figure 3.25 (c).*

Average horizontal dispersion value is remained constant when comparing the results by just effect of spouting gas velocity with the cases with effect of fluidizing velocity.

By increasing the ed length and fluidization velocity more uniform pattern of horizontal dispersion acheives.

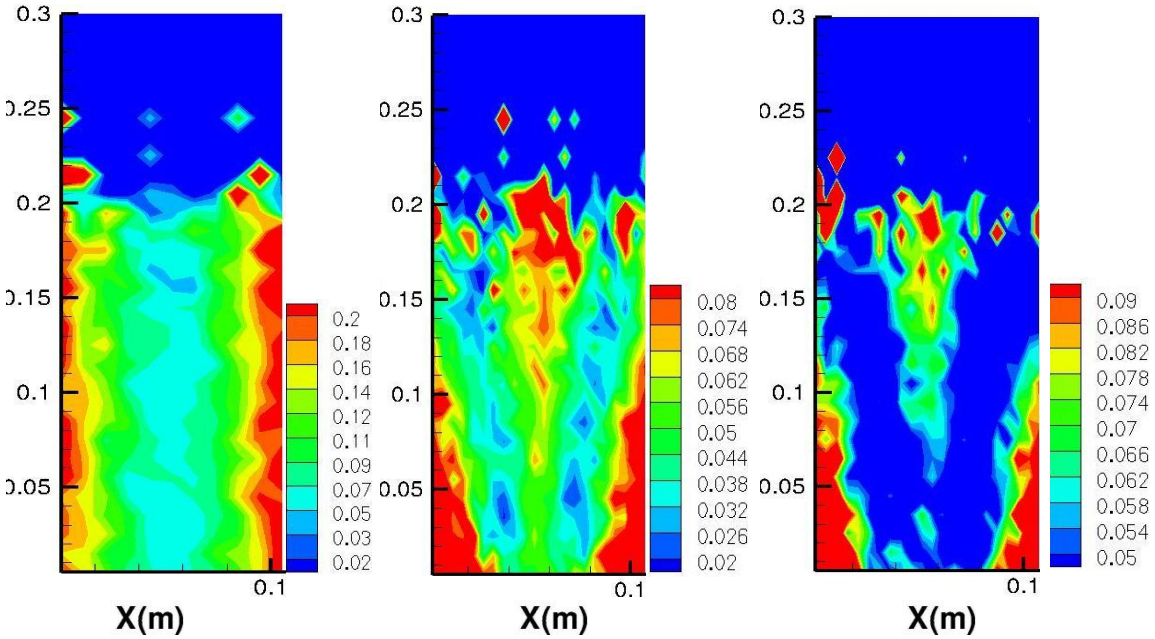

(a)U_f = 0.88 U_{mf} (b)U_f =1.15 U_{mf} (c)U_f = 1.33 U_{mf}

Figure 3.25 Horizontal dispersion with constant U_s/U_{ms}=1.1 and increasing fluidizing velocity in fluidized bed with width of 11 cm

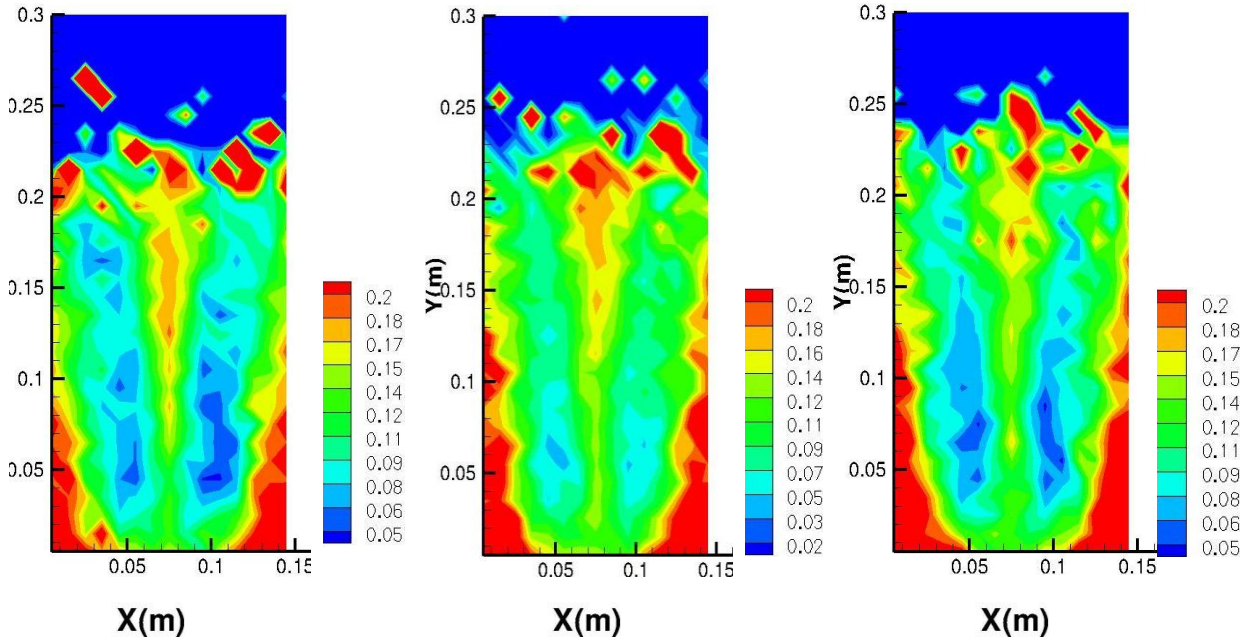

(a)U_f = 0.88 U_{mf} (b)U_f =1.15 U_{mf} (c)U_f = 1.33 U_{mf}

Figure 3.26 Horizontal dispersion with constant U_s/U_{ms}=1.1 and increasing fluidizing velocity in fluidized bed with width of 15 cm

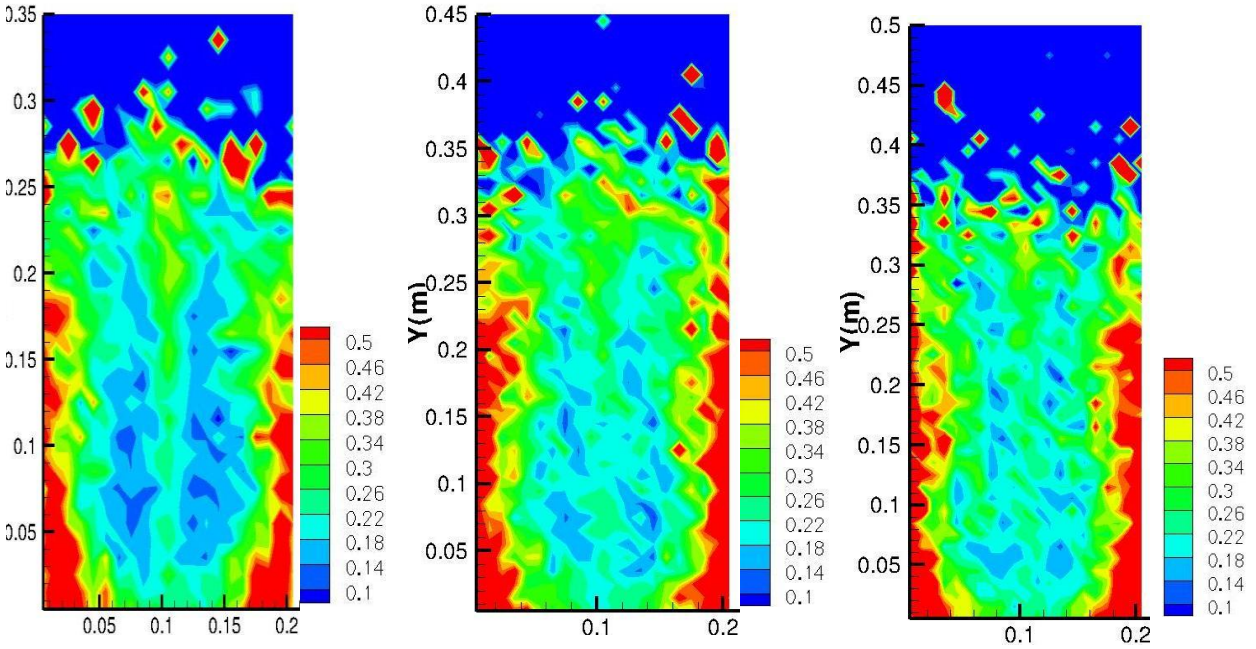

(a)U_f = 0.88 U_{mf} (b)U_f =1.15 U_{mf} (c)U_f = 1.33 U_{mf}

Figure 3.27 Horizontal dispersion with constant U_s/U_{ms}=1.1 and increasing fluidizing velocity in fluidized bed with width of 21 cm

4 Coclusion

In this master thesis, mono dispersed flatted-bottom spouted bed and fluidized beds simulated in MFIX software to investigate the mixing behavior of particles, preferential positions and velocity vectors. Also, horizontal dispersion in these beds in different conditions of bed width and spouted gas and fluidized gas velocities obtained. Dispersion is a significant parameter in determining the place of injection of fuel in the beds and understanding mixing criteria.

In this work, effect of bed widths (11cm, 15 cm and 21 cm) which simultaneously indicated change in the bed material is of concern. Effect of spouted gas velocity and fluidizing velocity was interesting parameter.

To better understand the distribution of particles through the bed, a sampling method defined and in specific locations of bed, distribution of tracer particles' concentration in axial and radial direction obtained. As the comparison of axial and radial distribution of tracers 'concentration was not easy, mixing index used to compare the uniformity of mixing in axial and radial direction.

Preferential position of particles is the pattern shows the tendency of particles to move across places in the bed during mixing. These patterns obtained based on different bed widths and various spouting and fluidizing gas velocities; therefore, velocity vectors were interesting to obtain. Velocity vectors showed two vortexes and one main bubble path in the two general feature of beds(fluidized and spouted beds) and parameters changing indicated with increasing bed length which means increasing in number of particles, also with increasing beds' gas velocity more significant and clear vortexes observable. In harmony with these patterns, horizontal dispersion in each case obtained and showed the movement and spreading of particles during mixing, through the bed.

For future work, it would be fruitful to change particles diameter that poly-dispersed particles be present in the beds. Also, different particles' density is desirable in the bed while the computational grid could be changed from single grid to multi grid, so that tracer particles or fuel particles could be tracked individually and more accurate results of mixing.

References:

1. Syamlal, M., Rogers, W., J. O'Brien T. (1993): *MFIX Documentation Theory guide, Technical Note,* U.S Department of Energy, Morgantown Energy Technology Center, DOE/METC-94/1004(DE94000087), Morgantown, West Virginia, December 1993.

2. Syamlal, M.(1998): *MFIX Documentation, Numerical Technique,* EG&G Technical Services of West Virginia Inc., U.S Department of Energy, Morgantown Energy Technology Center, DOE/MC31346-5824 (DE98002029), Morgantown, West Virginia, January 1998.

3. S. Boyalakuntla D. (2005): Simulation of Granular and Gas-Solid Flows Using Discrete Element Methods, Ph.D. Thesis, Department of Mechanical Engineering, Carnegie Mellon University, Pittsburgh, Pennsylvania, 2005, 184 pp.

4. Hoomans, B. P. B., Kuipers, J. A. M., van Swaaij, W. P. M., (2000): Granular Dynamics Simulation of Segregation Phenomena in Bubbling Gas-Fluidized Beds. *Powder Technology,* Vol. 109, No.1-3, April 2000, pp. 41-48.

5. Ginilaro, L.G., (2001): Fluidization-Dynamics**:** ***T****he Formulation and Applications of a Predictive Theory for the Fluidized State,* Butterworth-Heinemann, Oxford, 2001, 232 pp.

6. Kawaguchi, T., Tanaka, T., Tsuji, Y., (1998): Numerical Simulation of Two-Dimensional Fluidized Beds Using the Discrete Element Method (Comparison Between the Two-and Three-Dimensional Models). *Power Technology,* Vol. 96, No. 2, May 1998, pp. 129-138.

7. Deen, N.G., Sint Annaland, M., Van der Hoef, M.A., Kuipers, J.A.M., (2007): Review of Discrete Particle Modeling of Fluidized Beds, Chemical Engineering Science, Vol. 62, No. 1-2, January 2007, pp. 28-44.

8. Jie, L., Kuipers, J.A.M.(2003): Gas- Particle Interactions in Dense Gas-Fluidized Beds, Chemical Engineering Science, Vol. 58, No. 3-6, February-March 2003, pp 711-718.

9. WU, C., ZHAN, J., (2007): Numerical Prediction of particle Mixing behavior in a Bubbling Fluidized Bed. *Journal of Hydrodynamics*, Ser.B., Vol. 9, No. 3, June 2007, pp. 335-341.

10. R. Garg, J. Galvin, T. Li, S. Pannala(2010): Documentation of open-source MFIX–DEM software for gas-solids flows, From URL https://mfix.netl.doe.gov/documentation/dem doc 2010.pdf

11. Van Wachem, B.G.M, van der Schaaf J., Schouten J.C., Krishna R., van den Bleek C.M. (2001): Experimental Validation of Lagrangian-Eulerian Simulations of Fluidized Beds. *Powder Technology*, Vol. 116, No. 2-3, May 2001, pp. 155-165.

12. CRC Press (2006): *Multiphase Flow Handbook*, CRC Press, Boca Raton, FL., USA, 1156 pp.

13. Rhodes, M.J., Wang X.S., Nguyen M., Stewart P., Liffman K. (2001): Use of Discrete Element Method Simulation in Studying Fluidization Characteristics: Influence of Interparticle Force. *Chemical Engineering Science,* Vol. 56, No. 1, January 2001, 69-76 pp.

14. Mikami T., Kamiya H., Horio M., (1998): Numerical simulation of cohesive powder behavior in a fluidized bed. *Chemical Engineering Science,* Vol. 53, No. 10, May 1998, 1927-1940 pp.

15. Desai, N.(2003): *Invesitigation of gas-solid Multiphase Flow,* Ph.D. Thesis, Department of Mechanical Engineering, North Carolina State University, Raleigh, USA, 2003, 140 pp.

16. Garg, R., Narayanan C., Lakehal D., Subramaniam S., (2007): Accurate numerical estimation of intephase momentum transfer in Lagrangian-Eulerian simulation of dispersed two-phase flows. *International Journal of Multiphase Flow,* Vol. 33, No. 12, December 2007, 1337-1364 pp.
17. Sommerfeld, S., (1992): Modeling of particle-wall collision in confined gas-particle flows. *International Journal of Multiphase Flow,* Vol. 18, No. 6, November 1992, Pages 905-926 pp.

18. Zhang, D., Whiten, W.J. (1996): The calculation of contact forces between particles using spring and damping models. *Powder Technology,* Vol. 88, No. 1, July 1996, Pages 59-64 pp.

19. Tsuji, Y., Tanaka, T., Ishida, T., (1992): Lagrangian numerical simulation of plug flow of cohesionless particles in a horizontal pipe. *Powder Technology,*Vol. 71, No. 3, September 1992, Pages 239-250 pp.

20. Antonio, S., Suemi, R., (2009): Distance search techniques in quadtrees and octrees for random particle cluster simulations. *Proceedings of the 9th WSEAS International Conference on Systems Theory and Scientific Computation (ISTASC'09),* Stevens Point, Wisconsin, USA, 2009.

21. Muth, B., Muller, M., Eberhard, P., Luding, S.(2007): Collision Detection and Administration Methods for Many Particles with Different sizes. From URL: http://www.sfb716.uni-stuttgart.de/uploads/tx_vispublications/collision_detection_and_administration.pdf

22. Cambridge University Press (2004): *The Art of Molecular Dynamics Simulation*, Cambridge University Press, Cambridge, UK, 2004, 549 pp.

23. Oxford University Press (2002): *Computer Simulations of Liquids*. Oxford University Press, Oxford, UK, 2002.

24. Schinner, A., (1999): Fast algorithms for the simulations of polygonal particles, Springer, Vol.2, No. 1, DOI: 10.1007/s100350050032.

25. Yao. Z., Wang, J., Liu, G., Cheng, M.,(2004): Improved neighbor list algorithm in molecular simulations using cell decomposition and data sorting method. *Computer Physics Communications*, Vol. 161, No. 1-2, pp. 27-35.

26. J. Sadus, R., (2002): *Molecular Simulation of Fluids*, Elsevier Science, Amsterdam, The Netherlands, 2002, 515 pp.

27. Munjiza, A., Andrews, K.R.F.(1998): NBS contact detection algorithm for bodies of similar size. *International Journal for Numerical Methods in Engineering.* Vol. 43, No. 1, September 1998, pp. 131-149.

28. Gonnet, P. A., (2007): Simple Algorithm to Accelerate the Computation of Non-Bonded Interactions in Cell-Based Molecular Dynamics Simulations. *Journal of Computational Chemistry*, Vol. 28, No. 2, January 2007, pp. 570-573.

29. Zhang, Y., Jin, B., Zhong, W., (2009): Experiment on particle mixing in falt-bottom spout-fluid bed. *Chemical Engineering and Processing: Process Intensification*, Vol. 48, No., 1, January 2009, pp.126-134.

30. Marcel Dekker Inc. (2003): *Handbook of fluidization and Fluid-Particle Systems*, Marcel Dekker, USA, 2003, 850 pp.

31. Chaouki, J., Mostoufi, N., (2001): Local solid mixing in gas–solid fluidized beds. *Powder Technology*, Vol.114, No. 1-3, January 2003, pp. 23-31.

32. Chen, S.J., Fan, L.T,Watson, C.A.(1972): The mixing of solid particles in a motionless mixer-a stochastic approach. AIChE Journal, Vol. 18, No. 5, September 1972, pp. 984-989.

33. Farzaneh, M., Sasic, S., Almstedt A.E., (2010): A Novel Multigrid Approach for Lagrangian Modeling of Fuel Mixing in Fluidized Beds. *7th International Conference on Multiphase Flow ICMF 2010,* Tampa, FL USA, 2010.

34. Pallares D., Johnsson F., (2006): A novel technique for particle tracking in cold 2-dimensional fluidized beds- simulation fuel dispersion. *Chemical Engineering Science,* Vol. 61, No. 8, April 2006, pp. 2710-2720.

35. Monin, A.S., Yaglom A.M., (1975): *Statistical Fluid Mechanics: Mechanics of Turbulence,* MIT Press, Cambridge, USA, 1975, 882 pp.

36. Pismen, L.M., Nir, A., (1978): On the motion of suspended particles in stationary homogeneous turbulence. Journal of Fluid Mechanics, Vol. 84, January 1978, pp. 193-206.

37. Syamlal, M. (1997): Higher Order Discretization Methods for the Numerical Simulation of Fluidized Beds. *Fluidization and Fluid-Particle Systems Topical Conference, AIChE Annual Meeting,* Los Angeles, USA, 1997.

38. Guenther, C., Syamlal, M.(2001): *The Effect of Numericl Diffusion on Gas-Solids Fluidized Beds and the Use of Deferred Correction in a Finite Volume Method to Stabilize High Order Discretization of Convection Terms*, Scientific computing and applications, Nova Science Publisher Inc.,NY, USA, January 2001.

39. Prosperetti, A., Tryggvason G., (2007): *Computational methods for multiphase flow,* Cambridge University Press, Cambridge, UK, 2007, 466 pp.